Temporally precise single-cell-resolution optogenetics

Or A. Shemesh[1,2,3,4,5], Dimitrii Tanese[6], Valeria Zampini[6,7], Changyang Linghu[1,2,3,4,5], Kiryl Piatkevich[1,2,3,4,5], Emiliano Ronzitti[6,7], Eirini Papagiakoumou[6,8], Edward S. Boyden[1,2,3,4,5]* and Valentina Emiliani[6]*

Optogenetic control of individual neurons with high temporal precision within intact mammalian brain circuitry would enable powerful explorations of how neural circuits operate. Two-photon computer-generated holography enables precise sculpting of light and could in principle enable simultaneous illumination of many neurons in a network, with the requisite temporal precision to simulate accurate neural codes. We designed a high-efficacy soma-targeted opsin, finding that fusing the N-terminal 150 residues of kainate receptor subunit 2 (KA2) to the recently discovered high-photocurrent channelrhodopsin CoChR restricted expression of this opsin primarily to the cell body of mammalian cortical neurons. In combination with two-photon holographic stimulation, we found that this somatic CoChR (soCoChR) enabled photostimulation of individual cells in mouse cortical brain slices with single-cell resolution and <1-ms temporal precision. We used soCoChR to perform connectivity mapping on intact cortical circuits.

Optogenetics is in widespread use for the activation and silencing of populations of neurons defined by their molecular profiles, activity patterns or projection patterns[1]. Natural neural codes, however, vary from neuron to neuron even within a single class of cells, with neighboring neurons of the same type exhibiting potentially highly differing neural codes[2] and the firing of even single neurons capable of altering mammalian behavior or brain state[3,4]. Thus, an intriguing question is whether it is possible to drive individual neurons or sets of neurons with neuron-specific, distributed activity patterns exhibiting the temporal precision requisite to mimic natural neural codes.

Recently, interest has arisen around the topic of two-photon (2P) optogenetics, which as a result of the quadratic dependence of 2P excitation on light intensity and of the low scattering of infrared wavelengths, enables light to be targeted to single neurons at depth. 2P activation of opsins is robust at a biophysical level, with an excellent cross section for opsin photoactivation[5], but it is challenging to generate enough photo-evoked current using the micrometer-sized excitation volume of conventional 2P microscopy. Two primary strategies have been developed to increase the 2P illumination volume while keeping micrometer axial resolution: scanning and parallel. Scanning a laser spot, axially elongated to cover cell membranes, around a circular area with approximately the diameter of a cell body enables sequential excitation of channels, each contributing to the total induced photocurrent[5]. Scanning approaches, however, have

limited temporal resolution because of the time needed to sequentially scan the laser through multiple positions to cover a single cell body or multiple cells[6].

Parallel stimulation approaches such as generalized phase contrast[7] or computer-generated holography (CGH)[8] use phase modulation to precisely sculpt the illumination volume and simultaneously illuminate an entire cell or even multiple cells. In this case, simultaneous illumination of all channels enables efficient integration of light-evoked currents, allowing minimization of illumination time. In this condition action potentials can be generated with millisecond temporal resolution[7,9] and submillisecond temporal jitter[10,11]. Combined with temporal focusing, parallel stimulation also enables micrometer axial resolution and good preservation of axial resolution and spot shape after hundreds of micrometers of light propagation in scattering tissues[9,12,13]. CGH also enables 3D light generation[12,14–16], laying the groundwork for generating complex patterns with single-cell spatial resolution and millisecond temporal precision.

Advances in 2P stimulation methods, however, do not directly address the problem of cell bodies being densely surrounded by neurites of neighboring cells, whose membranes are separated by very thin gaps of extracellular space, smaller than the diffraction limit of light[17]. Thus, if neurons within a region bear densely expressed opsins, even 2P stimulation of a single neuron's cell body may excite opsins on dendrites or axons that are passing by, causing stray excitation of those nearby neurons. To address this crosstalk problem (Fig. 1a), we launched a screen to discover peptide sequences that could facilitate the localization of a high-photocurrent opsin to the cell body. We found that a short amino-terminal segment of the kainate receptor KA2 subunit[18], fused to the high-photocurrent channelrhodopsin CoChR[19], could enable the selective trafficking of CoChR to the cell body of neurons in the mammalian cortex (Fig. 1b), and, in combination with holographic 2P stimulation with a low-repetition fiber laser, this construct could support optogenetic stimulation of single cells in mammalian brain slices with <1-ms temporal resolution and with zero-spike crosstalk activation of nearby cells, using delivery of pulses of light of modest light powers. This fusion protein, which we call somatic CoChR (soCoChR), used in conjunction with optimized 2P stimulation approaches, may enable a diverse set of neural codes and computations to be probed in a causal fashion in systems and circuit neuroscience.

[1]Media Laboratory, Massachusetts Institute of Technology (MIT), Cambridge, MA, USA. [2]Department of Biological Engineering, MIT, Cambridge, MA, USA. [3]Center for Neurobiological Engineering, MIT, Cambridge, MA, USA. [4]Department of Brain and Cognitive Sciences, MIT, Cambridge, MA, USA. [5]McGovern Institute for Brain Research, MIT, Cambridge, MA, USA. [6]Neurophotonics Laboratory, Wave Front Engineering Microscopy Group, CNRS UMR8250, Université Paris Descartes, Paris, France. [7]Institut de la Vision, UM 80, UPMC, Paris, France. [8]Institut national de la santé et de la recherche médicale (Inserm), Paris, France. Or A. Shemesh, Dimitrii Tanese and Valeria Zampini contributed equally to this work. *e-mail: esb@media.mit.edu; valentina.emiliani@parisdescartes.fr

Results

Creation of a high-performance somatic opsin. We screened for soma-targeting sequences that could localize high-performance opsins to neuronal cell bodies. We first searched the literature for proteins that express somatically. We chose nine such proteins for consideration (Supplementary Table 1): myelin proteolipid proteins srPLP and
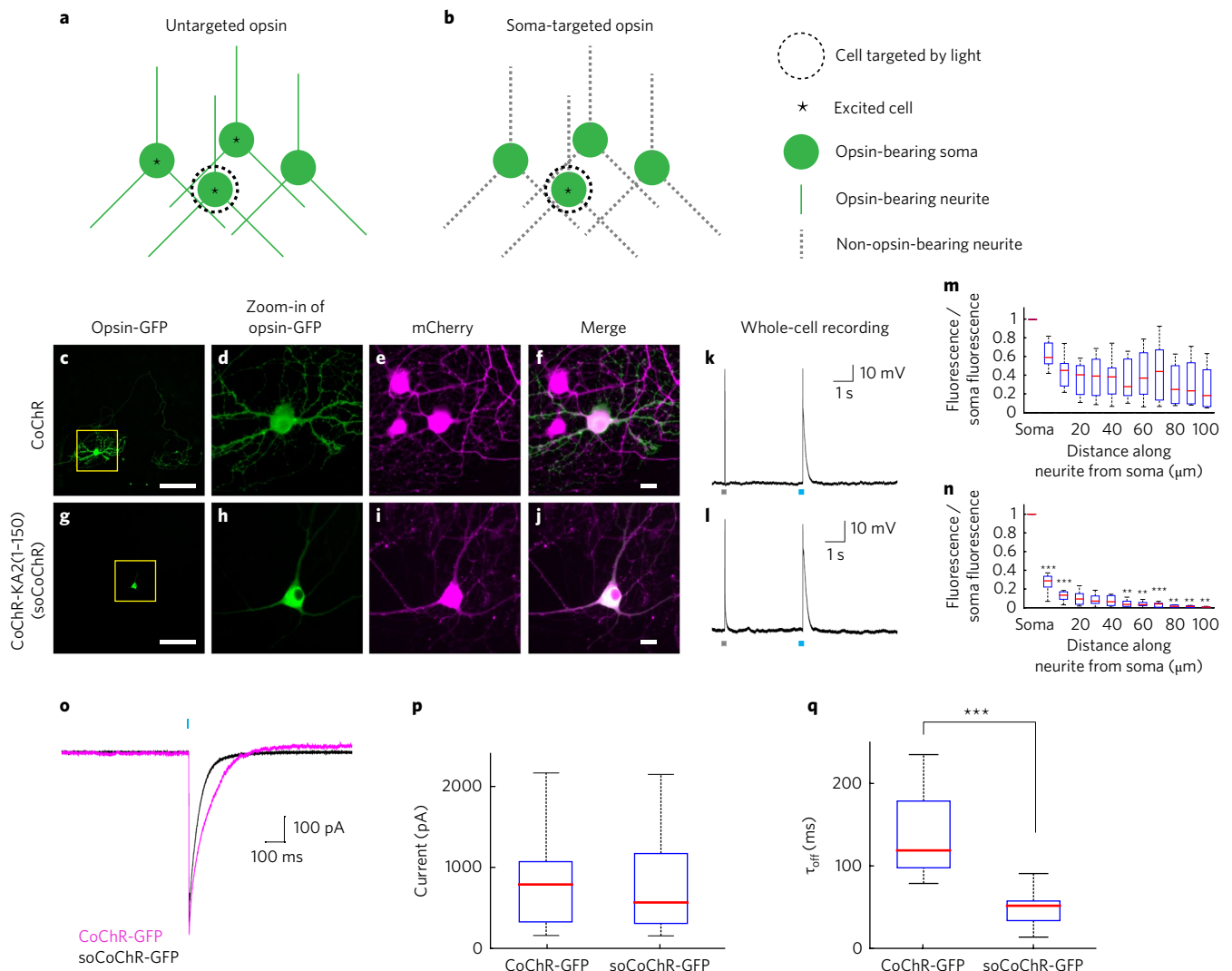

Fig. 1 | Soma-targeted optogenetics using the high-performance channelrhodopsin CoChR. a,b, Concept of soma-targeted optogenetics. Untargeted opsins, shown in **a**, express over the entire neural membrane. One can aim light at a given neural soma, but each cell body is surrounded by opsin-bearing neurites from other cells, resulting in artifactual activation of those cells. Restricting opsin expression to the cell body would prevent such side effects, enabling single-cell optogenetic stimulation, shown in **b**. **c–j,** Images are presented for cultured hippocampal neurons expressing wild-type vs. selectively trafficked CoChR fused to GFP, along with the cytosolic countermarker mCherry. **c,** A hippocampal neuron in culture expressing CoChR-GFP and mCherry, seen in the GFP channel (scale bar: 100 μm). **d,** Enlarged image from the yellow rectangle of **c**. **e,** The neuron from **c**, seen in the mCherry channel (magenta), along with surrounding neurons. **f,** Merge of **d** and **e** (scale bar for **d**–**f**: 20 μm). **g–j,** As in **c**–**f**, but for a neuron expressing CoChR-KA2(1–150)-GFP (soCoChR-GFP). **k,** Whole-cell current clamp recording of a cultured hippocampal neuron expressing CoChR-GFP, under current injection (10 ms duration; gray rectangle) and optical stimulation (480 nm, 34.84 mW/mm², 1 ms duration; blue rectangle). Rectangles not to scale. **l,** As in **k**, but for a neuron expressing soCoChR-GFP. **m,** Box-and-whiskers plot of GFP brightness versus position along a neurite, normalized to GFP brightness at the soma, extracted from neurites of cultured hippocampal neurons expressing CoChR-GFP ($n = 7$ neurites taken from 5 cells from 2 cultures). Red line denotes the median. Top and bottom edges of the box indicate the 75th and 25th percentiles, respectively. Top and bottom whiskers indicate the highest and lowest values, respectively. **n,** As in **m**, but for neurons expressing soCoChR-GFP ($n = 9$ neurites taken from 7 cells from 3 cultures). **$P < 0.01$ and ***$P < 0.001$, Bonferroni-corrected Kolmogorov–Smirnov test of brightness between wild-type and soma-targeted; see Supplementary Table 3 for full statistics. **o,** Representative photocurrents for cultured hippocampal neurons expressing CoChR-GFP (magenta) and soCoChR-GFP (black), under voltage clamp conditions, using 5-ms light pulses (480 nm, 34.84 mW/mm²; light blue rectangle). **p,** Box-and-whiskers plot (presented as in **m**) showing peak current amplitudes (pA) for CoChR-GFP and soCoChR-GFP in cultured hippocampal neurons illuminated with blue light (480 nm, 34.84 mW/mm², 5 ms; $n = 13$ neurons from 3 cultures and 13 neurons from 3 cultures for CoChR-GFP and soCoChR-GFP, respectively). Not significant; $P = 0.6444$; Wilcoxon rank sum test; see Supplementary Table 3 for full statistics. **q,** Box-and-whiskers plot (presented as in **m**) showing photocurrent decay time (τ_{off}, in milliseconds) for CoChR-GFP and soCoChR-GFP in cultured hippocampal neurons illuminated with blue light (480 nm, 34.84 mW/mm², 5 ms; $n = 13$ neurons from 3 cultures and 13 neurons from 3 cultures for CoChR-GFP and soCoChR-GFP, respectively). ***$P < 0.0001$; Wilcoxon rank sum test; see Supplementary Table 3 for full statistics.

DM20[20], the potassium channel $K_V2.1$[21], sodium channels $Na_V1.2$ and $Na_V1.6$[22], the adhesion molecule L1 with the soma-retention-causing mutation R184Q[23], the dynein adaptor protein Bicaudal-D (BicD) truncated after 50 codons (out of 782; this truncation impairs transport of fragile X mental retardation protein out of the soma)[24,25], the adaptor protein ankyrin G[26] and the kainate receptor subunit KA2[18].
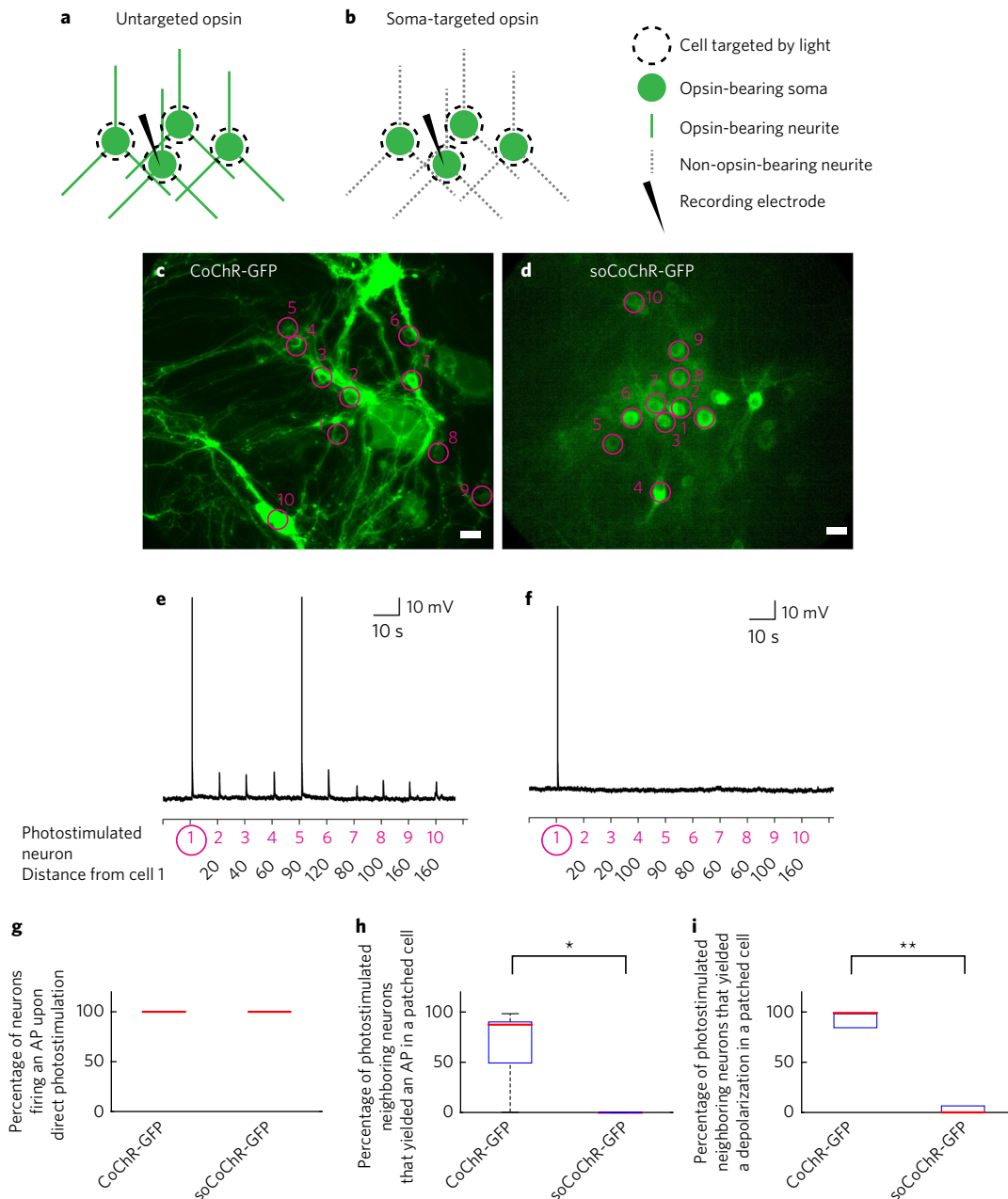

Fig. 2 | Zero-spike crosstalk single-cell optogenetic control of cultured neurons with 1P illumination. a,b, Schematic of the experiment. Cultured hippocampal neurons 2 weeks after transduction with AAV8-Syn-CoChR-GFP (untargeted CoChR, **a**) or AAV8-Syn-soCoChR-GFP (somatic soCoChR, **b**). One cell in the field of view was patched (current clamp). The patched cell along with nine neighboring cells were photostimulated consecutively using a digital micromirror device (DMD). **c**, Cultured hippocampal neurons expressing CoChR-GFP; regions of stimulation are highlighted by magenta circles. Numbers denote the order of stimulation. Scale bar: 20 μm. **d**, As in **c**, but for soCoChR-GFP. **e**, Representative current-clamp recording for a cultured hippocampal neuron expressing CoChR-GFP. Cells were photostimulated sequentially using the DMD (470 nm, 40.7 mW/mm², 1 ms light pulse). The order of photostimulation, as indicated by the numbers in **c**, is given on the x axis. The patched cell is numbered 1. The distance of cells 2–9 from the patched cell is given below each cell number in micrometers. **f**, As in **e**, but for soCoChR-GFP. **g**, Percentage of cultured hippocampal neurons that fired an AP upon direct photostimulation, using light pulses as above ($n=5$ cells from 4 cultures for CoChR-GFP; $n=5$ cells from 5 cultures for soCoChR-GFP). Red line denotes the median. **h**, Box-and-whiskers plot showing, averaged across all patched neurons, the percentage of photostimulated neighboring cells that yielded an AP in each patched cell ($n=5$ cells from 4 cultures for CoChR-GFP; $n=5$ cells from 5 cultures for soCoChR-GFP). Red line denotes the median. Top and bottom edges of the box indicate the 75th and 25th percentiles, respectively. Top and bottom whiskers indicate the highest and lowest values, respectively. *$P=0.0476$, Wilcoxon rank sum test; see Supplementary Table 3 for full statistics. **i**, Box-and-whiskers plot (presented as in **h**) showing, averaged across all patched neurons, the percentage of photostimulated neighboring cells that yielded a depolarization in each patched cell ($n=5$ cells, in 4 cultures for CoChR-GFP; $n=5$ cells, in 5 cultures for soCoChR-GFP). **$P=0.0079$, Wilcoxon rank sum test; see Supplementary Table 3 for full statistics.
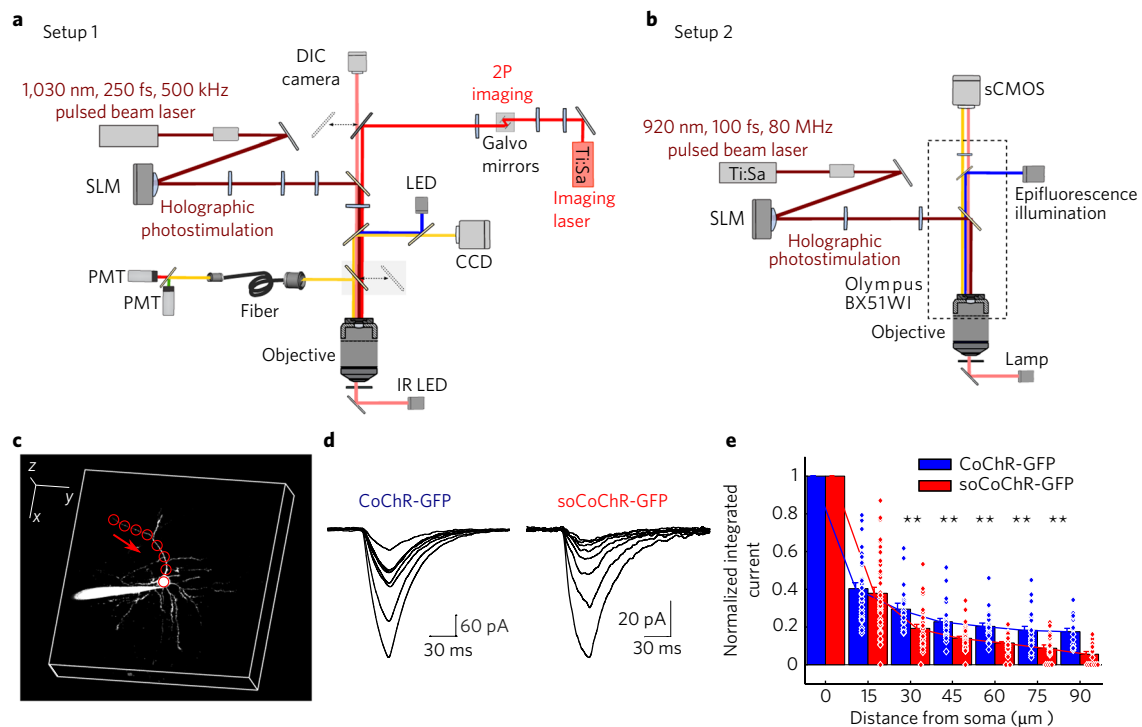
Fig. 3 | Photocurrents of neurites expressing soCoChR-GFP are significantly smaller than in neurites expressing CoChR-GFP, in neurons virally expressing these opsins in mouse cortical brain slices. a,b, Schematic representation of the two experimental setups used for holographic illumination. In setup 1, shown in **a**, holographic photostimulation was achieved using an amplified fiber laser and was coupled with a two-photon (2P) scanning imaging system. In setup 2, shown in **b**, holographic photostimulation was achieved using a conventional Ti:sapphire pulsed laser and was coupled with a widefield epifluorescence imaging system. See Methods and Supplementary Fig. 6. CCD, charge-coupled device; DIC, differential interference contrast; galvo, galvanometer; IR LED, infrared light-emitting diode; PMT, photomultiplier tube; sCMOS, scientific complementary metal-oxide semiconductor camera; SLM, spatial light modulator; Ti:Sa, titanium-sapphire laser. **c**, Schematic of 2P holographic stimulation along one neurite, showing Alexa 594 fluorescence (obtained via 2P scanning at 780 nm) from dye injected into a patched CoChR-GFP-expressing neuron. The Alexa 594 fluorescence was used to guide holographic spot placement (red circles) to different points along a neurite, at different distances from the soma. Red arrow indicates the order of photostimulation. The bright emission to the left of the cell represents the patch pipette filled with Alexa 594 (scale bars: 50 μm along all three axes; image acquired with setup 1). **d**, Representative whole-cell currents recorded from a CoChR-GFP-expressing neuron (left) and a soCoChR-GFP-expressing neuron (right; some 50 Hz electrical noise is apparent in the traces on the right), illuminated with a power density corresponding to the spiking threshold power density (18 μW/μm² and 101 μW/μm² for the CoChR-GFP- and the soCoChR-GFP-expressing cells, respectively; λ = 1,030 nm; setup 1). **e**, Bar plot of the integral of the elicited photocurrent, normalized to that obtained with the spot at the soma, as a function of distance from the soma, for CoChR-GFP-expressing (blue bars) and soCoChR-GFP-expressing (red bars) neurons (spacing between spots ~10 μm, λ = 1,030 nm or 920 nm for setup 1 or setup 2, respectively; data were pooled across the two setups). Bars reports mean ± s.e.m. Dots denote values for single neurites. For each cell, the photostimulation was done at the power density threshold determined for that cell (average powers: 29 ± 10 μW/μm² for CoChR-GFP-expressing cells, 90 ± 60 μW/μm² for soCoChR-GFP-expressing cells; power values refer to setup 1; see Methods). The normalized current integral was significantly higher in CoChR-GFP relative to soCoChR-GFP-expressing cells for distances of 30 μm or more from the soma. **P < 0.0017 for distances ≥30 μm; Kolmogorov–Smirnov test with Bonferroni correction (n = 16 neurites from 8 CoChR-GFP cells from 7 mice; n = 27 neurites from 16 soCoChR-GFP cells from 13 mice; see Supplementary Table 4 for full statistics).

In some studies, neuron somatic localization had been explored further by fusing the proteins to reporters: $Na_V1.2$, $Na_V1.6$, L1-R184Q and ankyrin G had previously been fused to fluorescent proteins[22,23,26], KA2 to a myc tag[18] and $K_V2.1$ to a hemagglutinin (HA) tag[21]. For some of the above soma-restricting proteins, fragments were shown to be sufficient to cause somatic targeting of a reporter (Supplementary Table 1). For each of $Na_V1.2$ and $Na_V1.6$, a 27-amino-acid segment within the intracellular loop between transmembrane domains II and III—termed $Na_V1.2$(II–III) and $Na_V1.6$(II–III), respectively—was sufficient[22]; for $K_V2.1$ a 65-amino-acid segment at the C terminus (here abbreviated Kv2.1-motif) sufficed[21,27]; for ankyrin G the N-terminal 837 amino acids of the protein sufficed[28]; and for BicD the N-terminal 50 amino acids located at locus r5 in the *Drosophila BicD* gene sufficed[25].

We fused GFP to full-length clones of the four soma-targeting proteins described above for which no sufficient fragment was reported (srPLP, DM20, L1-R84Q and KA2), as well as to the reported fragments for the other proteins (Supplementary Table 1). We transfected these GFP fusions into cultured hippocampal neurons and visually observed that three of the nine sequences tested appeared to target GFP primarily to the cell body (Supplementary Table 1).

We chose two of these three proteins for further consideration, KA2 and NaV1.2(II–III)-GFP (the third, ankyrin, was too large to easily be delivered in the AAV virus). Since KA2 is a 979-amino-acid protein and thus unwieldy from a viral packaging standpoint, we divided KA2 into three parts. This resulted in fragments (listed from N terminus to C terminus) of length 360 amino acids (containing one transmembrane domain[29]), 360 amino acids (containing three transmembrane domains) and 259 amino acids (containing one transmembrane domain and an arginine-rich endoplasmic reticulum retention sequence[30]). GFP fused to the first fragment was
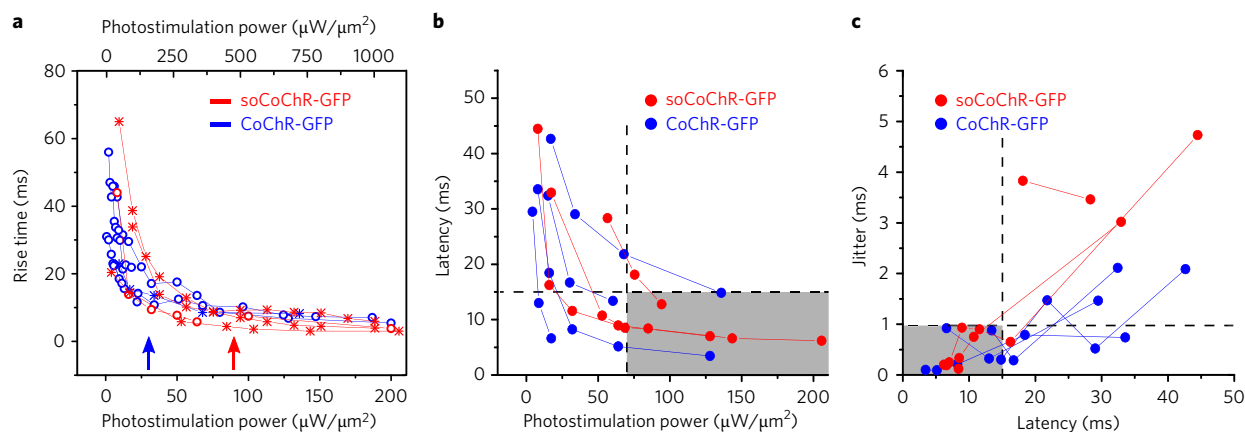
Fig. 4 | 2P power necessary to enable millisecond control of cortical neuron activation in mouse brain slice. a, Rise time of soCoChR-GFP-mediated (red) and CoChR-GFP-mediated (blue) photocurrents, measured in mouse brain slice cortical neurons, as a function of 2P stimulation power ($n = 4$–12 photostimulation powers per cell, 6 cells from 6 mice for CoChR-GFP; $n = 2$–11 photostimulation powers per cell, 5 cells from 5 mice for soCoChR-GFP). Data collected from setup 1 are plotted with circles and correspond to the power scale on the bottom x axis; data collected from setup 2 are plotted with asterisks and correspond to the top x axis. The length of the top x axis was rescaled with respect to the bottom x axis by a power conversion factor $k = 5.3$ (see Methods). Lines connect data acquired from the same neuron. Blue and red arrows indicate average threshold powers relative to setup 1 for CoChR-GFP- and soCoChR-GFP-expressing neurons, respectively (for CoChR-GFP: $28 \pm 10\,\mu W/\mu m^2$, $n = 7$ cells from 5 mice; for soCoChR-GFP: $83 \pm 39\,\mu W/\mu m^2$, $n = 4$ cells from 4 mice). **b**, The AP latency, defined as the time from the onset of 2P stimulation to the peak of the AP, plotted vs. 2P stimulation power in setup 1 units ($n = 3$–5 powers per cell for 4 cells from 3 mice for CoChR-GFP, blue dots; $n = 3$–5 powers per cell for 3 cells from 3 mice for soCoChR-GFP, red dots). Lines connect data acquired from the same neuron. Horizontal dashed line denotes 15 ms latency and vertical dashed line denotes $70\,\mu W/\mu m^2$ stimulation power, for comparison to **c**. Setups 1 and 2 were used interchangeably; power values used on setup 2 were scaled to equivalent power values for setup 1 (see Methods). See **c** for description of the gray area. **c**, AP temporal jitter (measured as s.d. of the AP latency across a series of 5 photostimulations for a given cell) plotted as a function of AP latency ($n = 3$–5 powers per cell for 4 cells from 3 mice for CoChR-GFP, blue dots; $n = 3$–5 powers per cell for 3 cells from 3 mice for soCoChR-GFP, red dots). Lines connect data acquired from the same neuron. Setups 1 and 2 were used interchangeably. Jitter below 1 ms (horizontal dashed line) was ensured when the latency was kept below 15 ms (vertical dashed line), corresponding to a photostimulation power higher than ~$70\,\mu W/\mu m^2$. The gray areas in **b** and **c** mark the region in which such conditions were satisfied.

somatic, but GFP fused to the latter two were not (Supplementary Table 1). We tried the N-terminal 150 amino acids of fragment 1, which we termed KA2(1–150), and found that this targeted GFP to the cell body (Supplementary Fig. 1 and Supplementary Table 2), but KA2(1–75) did not. As for NaV1.2(II–III), an earlier study[31] using this to target ChR2-YFP to the axon hillock of neurons revealed photocurrents smaller than those of ChR2-YFP[31], as well as alterations of neuron excitability[32], so we retained this motif for comparison purposes (Supplementary Fig. 2 and Supplementary Table 3) but did not pursue it further.

Key to efficient use of 2P light power for multicell activation is the presence of an opsin with high currents. Accordingly, we examined opsins that exhibited very high photocurrents but whose performance in intact mammalian brain circuitry had not yet been explored. We fused KA2(1–150) to the C terminus of CoChR, a powerful opsin with perhaps the largest photocurrent yet described[19], nearly an order of magnitude bigger than that of ChR2, at least when assessed in cultured neurons. We examined the resulting localization in cultured neurons, finding that, unlike wild-type CoChR-GFP (Fig. 1c–f), CoChR-KA2(1–150)-GFP (here called soma-targeted CoChR or soCoChR for short) appeared primarily at and near the cell body (Fig. 1g–j). Quantitatively, at $50\,\mu m$ from the edge of the cell body, CoChR-KA2(1–150)-GFP fluorescence was $4.67 \pm 1.29\%$ of the average brightness across the cell body, in contrast to $35.56 \pm 8.33\%$ for the wild-type opsin (mean $\pm$ s.e.m.; $n = 9$ neurites taken from 7 cells from 3 cultures for the KA2 fusion, $n = 7$ neurites taken from 5 cells from 2 cultures for the wild type; Fig. 1m,n). We found that, for most distances between 0 and $100\,\mu m$ from the edge of the cell body, in CoChR-KA2(1–150)-GFP-expressing cells the neurite fluorescence was significantly lower than in CoChR-GFP-expressing cells ($n = 9$ neurites from 7 cells from 3 cultures for CoChR-KA2(1–150)-GFP; $n = 7$ neurites from

5 cells from 2 cultures for CoChR-GFP; see Supplementary Table 3 for statistics).

As for the Kv2.1-motif sequence, which has been used by multiple groups to target ChR2 to the cell body[27,33], we found that the expression of CoChR-GFP-Kv2.1-motif was not purely at the cell body (Supplementary Fig. 3). Quantitatively, at $50\,\mu m$ from the edge of the cell body, CoChR-GFP-Kv2.1-motif fluorescence was $33.60 \pm 4.75\%$ of the average brightness across the cell body, whereas this ratio was $35.56 \pm 8.33\%$ for wild-type CoChR (mean $\pm$ s.e.m.; $n = 5$ neurites taken from 5 cells from 2 cultures for the Kv2.1-motif fusion, $n = 7$ neurites taken from 5 cells from 2 cultures for the wild type; Supplementary Fig. 3). Statistically, the brightness difference between CoChR-GFP and CoChR-GFP-Kv2.1 was not significant along neurites ($n = 5$ neurites from 3 cells from 2 cultures for CoChR-GFP-Kv2.1-motif; $n = 7$ neurites from 5 cells from 2 cultures for CoChR-GFP; see Supplementary Table 3 for Bonferroni-corrected Kolmogorov–Smirnov tests). Thus we chose not to further pursue CoChR-GFP-Kv2.1-motif.

CoChR-GFP and CoChR-KA2(1–150)-GFP could both mediate action potentials (APs) in neurons in response to blue light pulses (Fig. 1k,l). Photocurrent measurements (Fig. 1o,p; 5-ms light pulses at 480 nm, $34.84\,mW/mm^2$) revealed that CoChR-GFP and CoChR-KA2(1–150)-GFP had average photocurrents of $1{,}029 \pm 217$ pA and 720 ± 156 pA, respectively (mean $\pm$ s.e.m., $n = 13$ and 13 cells each from 3 and 3 cultures for CoChR-GFP and CoChR-KA2(1–150)-GFP, respectively; Supplementary Table 3). As previously reported[19], CoChR-GFP under single-photon (1P) widefield activation has a long photocurrent decay time (Fig. 1q; $\tau_{off} = 150 \pm 18$ ms, where value is mean $\pm$ s.e.m.). This value was shorter for CoChR-KA2(1–150)-GFP (52 ± 6 ms; mean $\pm$ s.e.m.; $n = 13$ neurons from 3 cultures, 13 neurons from 3 cultures for CoChR-GFP and CoChR-KA2(1–150)-GFP, respectively; Fig. 1q; see Supplementary Table 3),

perhaps because in the latter case the patch pipette is not recording the currents that propagate in from distant neurites when a wild-type opsin is illuminated.

Using CoChR- and soCoChR-expressing cultured neurons, we measured the action spectra of these molecules (Supplementary Fig. 4a), the spike probability (Supplementary Fig. 4b) and photo-current (Supplementary Fig. 4c) mediated by these molecules as a function of irradiance, and the spike fidelity mediated by these molecules as a function of the stimulation frequency (Supplementary Fig. 4d). We also examined basic cell health parameters. The passive membrane properties for neurons containing CoChR-GFP ($n = 10$ cells from 3 cultures) vs. CoChR-KA2(1–150)-GFP ($n = 10$ cells from 3 cultures) were not significantly different ($P > 0.05$, Kruskal–Wallis test for these membrane properties: resting potential, membrane capacitance, holding current and membrane resistance; see Supplementary Fig. 5).

Somatic CoChR enables single-cell optogenetic control using 1P photostimulation. To test whether soCoChR-GFP could mediate 1P stimulation of cultured neurons without stimulating nearby cells, we patched a single cell under widefield fluorescence microscopy and used a digital micromirror device (DMD) to photostimulate the patched cell and its neighbors with 20-μm-diameter spots (Fig. 2a,b) under synaptic blockade. For cells expressing either CoChR-GFP or soCoChR-GFP ($n = 5$ for both opsins; average distance of photostimulated cell from patched cell = 76.89 ± 6.98 μm and 74.22 ± 6.50 μm, respectively; Fig. 2c,d and Supplementary Table 3), illuminating the cell body of the patched cell as described in Fig. 2e always yielded an AP in that cell. Furthermore, while patching a CoChR-GFP-expressing cell and photostimulating the somata of neighboring (i.e., non-patched) CoChR-GFP-expressing cells, we recorded an AP when photostimulating $62.0 \pm 16.3\%$ of the neighboring cells (Fig. 2e,h; mean ± s.e.m.; $n = 5$ patched cells from 4 cultures); in contrast, while patching a soCoChR cell, photostimulating the neighboring cells' somata never resulted in an AP in the patched cell ($P < 0.01$, Wilcoxon rank sum test; Fig. 2f–h; $n = 5$ patched cells from 5 cultures). Analyzing the data further, we found depolarizations of >0.5 mV above baseline (defined as the average voltage over the 100 ms preceding the voltage change; see Methods) in patched cells within CoChR-GFP-expressing networks when $96.0 \pm 2.4\%$ of the nearby cells were stimulated (Fig. 2e,i; mean ± s.e.m.), in contrast to when $4.0 \pm 4.0\%$ of the nearby-cell stimulations for soCoChR-expressing neural networks ($P < 0.001$, Wilcoxon rank sum test; Fig. 2f,i; mean ± s.e.m.).

Two-photon holographic control of soCoChR-expressing neurons in brain slice. We next sought to assess the potential for soCoChR to mediate single-cell optogenetic control in intact mouse brain slices. The strong scattering of visible light in tissue will induce a broadening of the excitation spot and therefore spurious activation of distant neurons by both out-of-focus and scattered photons[34,35]. To avoid this possibility we used 2P activation, and to optimize temporal resolution we used parallel holographic light illumination. We implemented holographic 2P activation in two different microscopes (Fig. 3a,b and Supplementary Fig. 6). In setup 1, we combined a custom-made 2P scanning system with a 2P CGH setup, using a low-repetition-rate amplified fiber laser ($\lambda = 1{,}030$ nm; exit average power = 10 W; repetition rate = 500 kHz; pulse duration = 250 fs) as the excitation source. In setup 2, we combined a 1P epifluorescence microscope with a 2P CGH system using as the excitation source a conventional mode-locked Ti:sapphire femtosecond laser ($\lambda = 920$ nm; exit average power = 1.6 W; repetition rate = 80 MHz; pulse duration = 100 fs). Setup 1 was designed to achieve simultaneous activation of multiple cells, since the high output power and low repetition rate of the laser source enabled parallel illumination with high-energy pulses while keeping average power low. Setup 2,

in contrast, had lower output power and used conventional and commonly available laser sources. The tunable laser source used in setup 2 enabled us to tune the excitation wavelength to the peak of the 2P spectrum (Supplementary Fig. 7), while the laser source used in setup 1 has a fixed excitation wavelength of 1,030 nm, which elicits a current of magnitude ~50% of that at the excitation peak (Supplementary Fig. 7).

We quantified the spatial confinement of soCoChR vs. CoChR by measuring the photostimulated current integral while steering a 10-μm-diameter holographic spot away from the soma of a patched neuron in ~10-μm steps along a neurite, using a mouse cortical brain slice in the presence of synaptic receptor blockers (NBQX, gabazine, strychnine, APV) (Fig. 3c,d). 2P photostimulation power density was set, for each cell, at the minimum value necessary to reliably (in each of three consecutive trials) trigger one AP using a 30-ms photostimulation pulse illuminating the whole soma (threshold power for CoChR-GFP: 28 ± 10 μW/μm^2 and 92 ± 93 μW/μm^2 using setups 1 and 2, respectively, $n = 7$ cells from 5 mice in setup 1 and $n = 10$ cells from 8 mice in setup 2; threshold power for soCoChR-GFP: 83 ± 39 μW/μm^2 and 261 ± 190 μW/μm^2 using setups 1 and 2, respectively, $n = 4$ cells from 4 mice in setup 1 and $n = 9$ cells from 6 mice in setup 2). The difference in power required for the two opsins may be due to a difference in expression efficiency for the two opsins in vivo. We cannot exclude the possibility that with the axial resolution used in the experiment (20–40 μm; Supplementary Fig. 8), neurites surrounding a given cell body contribute to the observed current, this effect being more pronounced for the non-soma-targeted opsin. For each illumination position along each neurite, we normalized the measured current integral to the corresponding value measured at the soma (Fig. 3e). The normalized current integral decayed more sharply along neurites expressing soCoChR-GFP than along neurites expressing CoChR-GFP ($P < 0.01$ at sites 30 μm from soma and beyond; $n = 16$ neurites from 8 CoChR-GFP cells from 7 mice; $n = 27$ neurites from 16 soCoChR-GFP cells from 13 mice). We note that the sharper current decay was observed even though for soCoChR-GFP we used higher photostimulation powers than for CoChR-GFP. Absolute values of currents corresponding to Fig. 3e are reported and analyzed in Supplementary Fig. 10 and Supplementary Table 4; the decay of the fluorescence of GFP (fused to the opsin) along the neurites is shown in Supplementary Fig. 9. Thus, photo-evoked currents fell off more rapidly along soCoChR-bearing neurites than those bearing CoChR, a crucial condition to support neuronal stimulation with single-cell resolution.

Millisecond-timescale activation of neurons in brain slices. We next searched for illumination conditions that enabled the triggering of APs with <1-ms temporal jitter in cells expressing soCoChR-GFP vs. CoChR-GFP. We measured the rise time (τ_{on}) and decay time (τ_{off}) of photocurrents generated by a holographic spot covering the cell body of an opsin-expressing neuron while we varied illumination power. For both CoChR-GFP- and soCoChR-GFP-expressing neurons, τ_{on} decreased with increasing illumination power (Fig. 4a), reaching an asymptotic value (see Methods) of 5.7 ± 2.6 ms in CoChR-GFP-expressing cells ($n = 4$ cells from 4 mice) and 4.1 ± 2.5 ms in soCoChR-GFP-expressing cells ($n = 4$ cells from 4 mice). τ_{off} values were independent of the illumination power and equal to 37 ± 13 ms in CoChR-GFP-expressing cells ($n = 4$ cells out of 4 mice) and 33.3 ± 5.6 ms in soCoChR-GFP-expressing cells ($n = 4$ cells out of 4 mice). Notably, these numbers were similar, in contrast to what was seen for 1P widefield illumination in cultured neurons (Fig. 1q), suggesting that restricting light illumination to the soma effectively equalized the decay times of photo-evoked currents for targeted vs. non-targeted opsins.

As a next step in understanding the temporal properties of 2P CGH excitation of soCoChR-bearing neurons, we assessed how AP
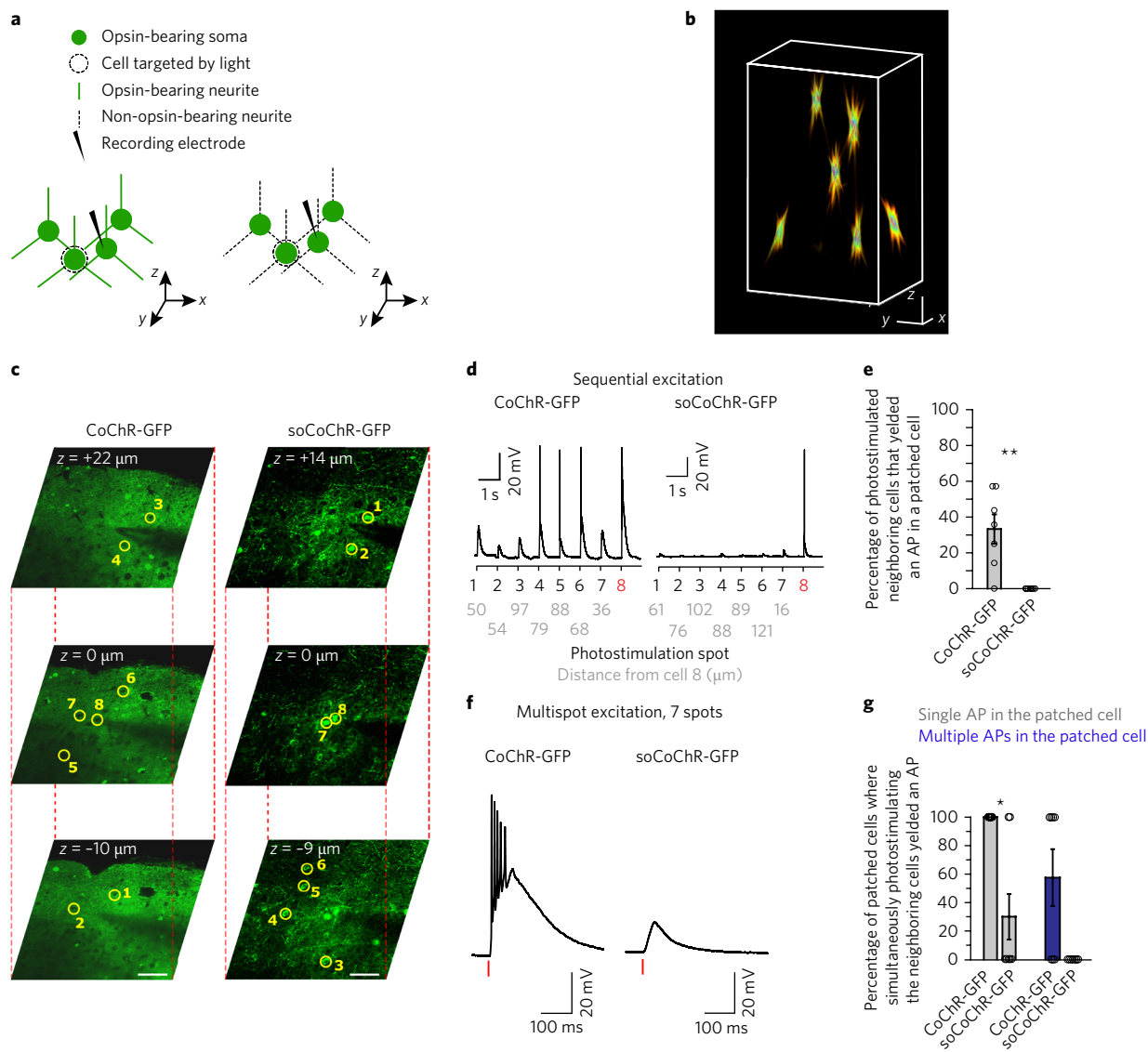
Fig. 5 | Soma-targeted CoChR enables single-cell control with 3D photoactivation in brain slices. a, Schematic of 3D holographic activation. One cell expressing CoChR-GFP or soCoChR-GFP was patched and then neighboring cells in different z-planes were illuminated with 10–14 µm diameter holographic spots. **b**, Reconstruction of multi-spot 3D holographic pattern obtained by measuring induced fluorescence from a thin layer of rhodamine 6 G (spin-coated on a glass coverslip), imaged through a second microscope objective; spot diameter 10 µm. Scale bars: 35 µm along all three axes. **c**, 2P images (imaging $\lambda = 920$ nm) from a 3D z-stack used to draw 10–14 µm holographic spots ($\lambda = 1,030$ nm, setup 1) on neighboring cells expressing CoChR-GFP (left, yellow circles numbered 1–7) or soCoChR-GFP (right, yellow circles numbered 1–7) and on the patched cell (yellow circle, numbered 8) inside a volume of approximately $200 \times 200 \times 70$ µm³ (scale bars: 50 µm). **d**, Whole-cell recording of a CoChR-GFP-expressing cell (left) and a soCoChR-GFP-expressing cell (right) while sequentially positioning the holographic spot on neighboring cells one at a time (represented in **c**; $\lambda = 1,030$ nm, setup 1, photostimulation power 100 µW/µm² for CoChR-GFP and for soCoChR, 30 ms duration). The distance of cells 1–7 from the patched cell 8 is given below each cell number in gray. **e**, Bar plot showing the percentage of neighboring cells that, when stimulated, yielded an AP in a given patched cell (and averaged across all patched cells; $n = 7$ cells from 6 mice for CoChR-GFP; $n = 7$ cells from 7 mice for soCoChR-GFP; values are mean ± s.e.m.). Dots denote values for single cells. $\lambda = 1,030$ nm, setup 1, average photostimulation power: CoChR-GFP 142 ± 24 µW/µm², soCoChR-GFP 173 ± 26 µW/µm²; 30 ms duration. **$P < 0.01$, Wilcoxon rank sum test ($P = 0.004$). **f**, Whole-cell recording of a CoChR-GFP-expressing cell (left) and a soCoChR-GFP-expressing cell (right; both cells presented in **d**) during simultaneous photostimulation of the neighboring cells represented in **c**, without a stimulation spot on the soma of the patched cell. Photostimulation power density for each spot was equal to the one used in **d** ($\lambda = 1,030$ nm, setup 1, photostimulation power 100 µW/µm² for CoChR-GFP and for soCoChR-GFP; 30 ms duration, red dash under traces). **g**, Bar plot showing the percentage of simultaneous photostimulations of neighboring cells that yielded APs in a given patched cell (averaged across all patched cells). Gray bars indicate the generation of 1 AP; blue bars indicate the generation of more than one AP ($n = 7$ cells expressing CoChR-GFP from 6 mice; $n = 7$ cells expressing soCoChR-GFP from 7 mice). Values are mean ± s.e.m. Dots denote values for single cells. $\lambda = 1,030$ nm, setup 1, average photostimulation power: 142 ± 24 µW/µm² and 173 ± 26 µW/µm² for CoChR-GFP-expressing cells and for soCoChR-GFP-expressing cells, respectively; 30 ms duration. For generation of one AP: *$P < 0.05$; χ^2 test ($\chi^2 = 3.97$, $P = 0.046$, d.f. $= 1$). For generation of more than one AP: $P = 0.08$, $\chi^2 = 3.15$, d.f. $= 1$. Average distances between patched cells and neighboring cells are reported in Supplementary Fig. 12 and Supplementary Table 4.
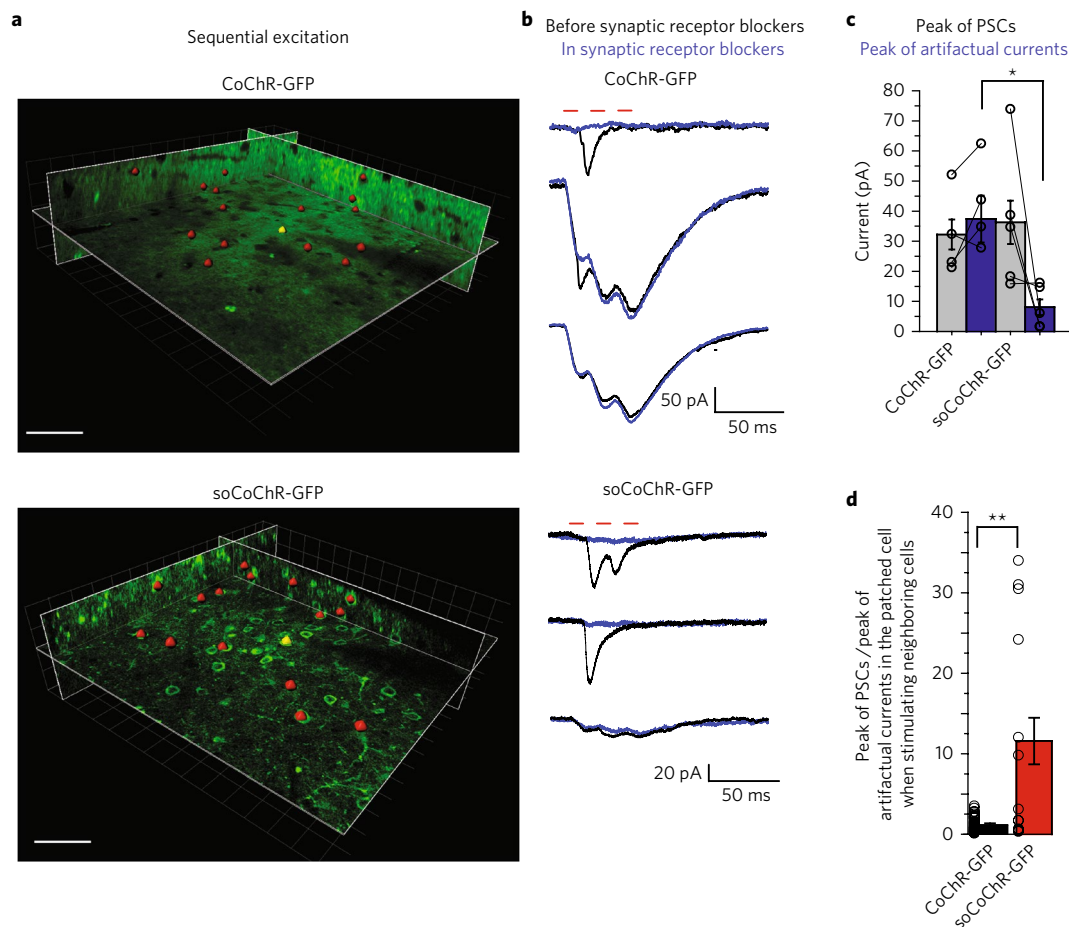
Fig. 6 | 2P holographic stimulation of soCoChR enables mapping of functional connectivity in brain slices. a, Schematic of the connectivity experiment: a 2P image ($\lambda = 920$ nm, setup 1) of the volume around a patched opsin-positive cell (yellow spot) expressing CoChR-GFP (top) or soCoChR-GFP (bottom) is used to sequentially position a 10–14 µm holographic spot (red spots) on nearby opsin-expressing cells and to calculate the corresponding phase masks. Scale bar: 40 µm. **b**, Representative currents recorded in whole-cell configuration from a CoChR-GFP-expressing (top) or soCoChR-GFP-expressing (bottom) cell while sequentially positioning the holographic spot on neighboring cells. Red bars represent the photostimulation periods for each cell (three light pulses at 50 Hz of 10 ms duration). Photostimulation power: 120 µW/µm² for CoChR-GFP; 150 µW/µm² for soCoChR-GFP; $\lambda = 1,030$ nm, setup 1. Black traces: currents recorded before the perfusion of receptor blockers (average of three trials on each spot position). Blue traces: artifactual currents recorded after the perfusion of receptor blockers (average of three trials on each spot position). **c**, Bar plots showing the peak amplitudes of postsynaptic currents sensitive to receptor blockers (PSCs; gray bars) and the peak amplitudes of artifactual currents recorded after the perfusion of receptor blockers (I_{ART}, blue bars) ($n = 4$ CoChR-GFP cells from 4 mice; $n = 5$ soCoChR-GFP cells from 5 mice). Currents were recorded in whole-cell configuration from cells expressing CoChR-GFP or soCoChR-GFP while sequentially positioning the holographic spot on neighboring cells one at a time ($\lambda = 920$ or 1,030 nm, setup 1 or 2; photostimulation power (relative to setup 1): 130 ± 30 mW/µm² for CoChR-GFP and 180 ± 20 mW/µm² for soCoChR-GFP; three light pulses at 50 Hz of 10 ms duration). For mean peak current comparison, *$P = 0.015$; Wilcoxon rank sum test. Bars report mean ± s.e.m. **d**, Bar plots showing the ratio PSC/I_{ART} ($n = 54$ out of 78 photostimulated neighboring cells triggering PSCs in the patched cell from 4 CoChR-GFP cells from 4 mice; $n = 15$ out of 109 photostimulated neighboring cells triggering PSCs in the patched cell from 5 soCoChR-GFP cells from 5 mice). Currents were recorded in whole-cell configuration from cells expressing CoChR-GFP or soCoChR-GFP while sequentially positioning the holographic spot on neighboring cells one at a time ($\lambda = 920$ or 1,030 nm, setup 1 or 2; photostimulation power (relative to setup 1): 130 ± 30 mW/µm² for CoChR-GFP and 180 ± 20 mW/µm² for soCoChR-GFP; three light pulses at 50 Hz of 10 ms duration). For comparison of ratio PSC/I_{ART}: **$P = 0.003$; Wilcoxon rank sum test. Bars report mean ± s.e.m.

latency (defined as the time interval between the onset of photoactivation and the peak of the AP) and AP jitter (defined as the standard deviation of the aforementioned latency) depended on the illumination power, for both wild-type CoChR and soCoChR. Increasing the photostimulation power density to values above 70 µW/µm² on setup 1 or 360 µW/µm² on setup 2 enabled, for both CoChR-GFP- and soCoChR-GFP-expressing neurons, a spike latency below 15 ms (Fig. 4b) and a spike jitter below 1 ms (Fig. 4c).

Single-cell activation of soCoChR-bearing neurons in brain slices using 3D holography. We assessed whether soCoChR-bearing neurons in combination with 2P holographic stimulation could

enable millisecond-precision single-cell optogenetics in brain slices. We performed crosstalk experiments as before, patching an opsin-expressing neuron and attempting to activate both the patched neuron and nearby neurons (Fig. 5a; experiments done using setup 1). We patched an opsin-expressing neuron, with synaptic transmission blocked, and acquired a 2P image stack to reconstruct the 3D volume ($\sim 200 \times 200 \times 80$ µm³) surrounding the patched cell. 3D holographic illumination allowed us to sequentially or simultaneously target multiple locations in such a volume (Fig. 5b). We randomly selected five to eight neighboring neurons in this volume (Fig. 5c). We then sequentially illuminated these cells with a 10–14 µm holographic spot while recording from the patched cell.

We used excitation powers above $70\,\mu W/\mu m^2$ that, accordingly to Fig. 4, ensure <15-ms latency and <1-ms jitter. In each sequence, for both CoChR-GFP or soCoChR-GFP, the patched cell responded with at least one AP when the holographic spot was placed on its cell body. For CoChR-GFP-expressing cells, in $33 \pm 8\%$ of the cells near a patched cell ($n = 7$ patched cells from 6 mice; Fig. 5d,e), illumination evoked an AP in the patched cell, whereas for soCoChR-GFP-expressing cells, illumination of neighboring cells one at a time never evoked an AP in the patched cell ($P < 0.01$; $n = 7$ patched cells from 7 mice; Fig. 5d,e). Thus, soCoChR used in combination with 2P CGH illumination could ensure zero-spike crosstalk, single-cell stimulation of neurons in intact brain circuitry, with <1-ms jitter of the resultant spikes.

Although individually illuminating neighboring soCoChR-GFP-expressing cells did not evoke APs in the patched cell, the illumination still induced an average crosstalk depolarization of $2.6 \pm 1\,mV$ in the patched cell (Fig. 5d; $n = 7$ cells from 7 mice). Accordingly, we assessed whether simultaneous stimulation of multiple neighboring cells could push a patched neuron to fire one or more APs, by exciting between five and eight randomly selected neighboring cells. We generated multiple spots, each with power density equal to the one used for the corresponding experiment with sequential cell stimulation ($142 \pm 24\,\mu W/\mu m^2$ and $173 \pm 26\,\mu W/\mu m^2$ for CoChR-GFP- and soCoChR-GFP-expressing cells, respectively; see also Methods and Supplementary Fig. 11). For CoChR-GFP, in 57% of the cells we observed multiple APs ($n = 7$ patched cells from 6 mice; Fig. 5f,g). In contrast, for soCoChR-GFP we never observed multiple APs ($n = 7$ patched cells from 7 mice; Fig. 5f,g). However, single APs were observed in 100% and 33% of patched cells for CoChR-GFP and soCoChR-GFP, respectively ($n = 7$ cells from 6 mice and 10 cells from 9 mice, respectively) in the simultaneous excitation condition.

These experiments were done at a power just below saturation (Supplementary Fig. 8d). This enabled us to assure a high enough channel recruitment without too much broadening of the axial resolution (Supplementary Fig. 8d) and consequently helped minimize artifactual out-of-focus neurite activations.

Finally, we performed local functional connectivity experiments in layer II/III of mouse primary visual cortex in brain slices. To this end, we patched a neuron expressing CoChR-GFP or soCoChR-GFP and then selected 15–25 neighboring opsin-positive cells in a volume of about $200 \times 200 \times 70\,\mu m^3$ centered on the patched cell (Fig. 6a,b and Supplementary Fig. 13). We then sequentially stimulated the neighboring cells (three 10-ms laser pulses at 50 Hz) while recording the currents in the patched cell (Fig. 6a,b) and repeated the entire sequence three times. To trigger APs with short (<10 ms) latency and millisecond jitter in the presynaptic cells, we applied laser powers in the range of $130 \pm 30\,\mu W/\mu m^2$ for CoChR-GFP and $180 \pm 20\,\mu W/\mu m^2$ for soCoChR-GFP (Fig. 4b,c). In both preparations, we repeated the same experiment in presence of synaptic receptor blockers (NBQX, gabazine, strychnine, APV) so that we could isolate the synaptic vs. artifactual components.

When performing the experiments in soCoChR-GFP-expressing cells, we found that $13 \pm 7\%$ of photostimulated neighboring cells evoked currents, here designated I_{TOT}, in the patched cell. The application of synaptic receptor blockers left a residual current ($8 \pm 6\,pA$; Fig. 6c and Supplementary Table 5) that corresponded to the artifactual component (designated I_{ART}), which came from the direct stimulation of dendrites or axons of the patched cell crossing the photostimulation volume. The component sensitive to receptor blockers ($I_{TOT} - I_{ART}$) was thus an estimate of the true postsynaptic current (PSC) ($36 \pm 16\,pA$; Fig. 6c).

In the case of CoChR-GFP-expressing cells, $71 \pm 14\%$ of photostimulated neighboring cells evoked currents, I_{TOT}, in the patched cell with an artifactual component, I_{ART}, of $37 \pm 15\,pA$, which was of about the same order as the PSC ($32 \pm 10\,pA$). These results revealed for CoChR the presence of a strong artifactual contribution. Overall, the ratio between the real PSCs and the artifactual peak currents was significantly higher in soCoChR-GFP-expressing cells compared to the case of CoChR-GFP-expressing cells (11 ± 10 in soCoChR-GFP; 1.4 ± 1.2 in CoChR-GFP; Fig. 6d and Supplementary Table 5).

Discussion

We here demonstrate that optical activation of single cells in dense mammalian neural circuitry, with <1-ms temporal jitter, is possible without causing stray spiking in neighboring neurons. We achieved this combined temporally and spatially precise optogenetics through molecular engineering—creating a soma-targeted version of the powerful opsin CoChR[19], or soCoChR for short, as well as optimal 2P holographic control of individual neurons. We screened potential trafficking sequences from nine different soma-localized molecules, first testing entire molecules as well as fragments with GFP and then CoChR. The first 150 amino acids on the N terminus of the kainate receptor subunit 2 enabled efficient targeting of CoChR to the soma, restricting CoChR expression to the first 20–50 μm of dendrites and axons, without alteration of cellular function. We showed that we could obtain zero-spike crosstalk 2P excitation of individual cells—that is, without driving APs in neighbors—but activating many neighbors at once could cause a nearby neuron to be excited to the point of spiking. This remaining multicellular activation crosstalk thus provides an avenue for future investigation.

We performed local functional connectivity experiments in cortical slices and showed that soma-targeted opsins enabled identification and measurement of postsynaptic currents in downstream cells. It is important to note that although the use of soma-targeted CoChR enabled a significant reduction in the artifactual component arising from the direct stimulation of postsynaptic cell processes, this contribution was not completely eliminated. Further improved soma-targeting strategies combined with improved axial confinement of the excitation volume—for example, by combining CGH[12] with temporal focusing (Supplementary Fig. 8f,g)—should enable further reductions in this artifactual component.

Optogenetic analysis of synaptic connectivity has been demonstrated before in intact mammalian circuits[36,37]. To avoid artifactual components in the PSCs, some previous studies have used expression of opsins in the presynaptic cell only, thereby ensuring that the postsynaptic cells do not contain an opsin[38]. Alternative strategies have used sparse labeling of the ChR2-expressing neurons[39] or selective opsin expression in a specific subset of neurons[40]. Pioneering experiments have used ChR2 targeted to the soma through $K_v2.1$[30,36] together with 1P[36] and 2P[33] activation. In the latter case, the authors were able to show the use of somatic opsins to map neuronal connectivity. However, these first experiments required long photostimulation pulses (150 ms) and used relatively high excitation power (~180 mW/cell)[33], which corresponded to a jitter of 17 ms. Thus, earlier efforts had limits on both the maximum number of targets (two to five) that could be simultaneously reached and the precision of the temporal control of spike generation.

Here we demonstrate that using somatic CoChR enables control of neuronal firing using short illumination pulses (10–30 ms) with temporal jitter short enough (<1 ms) to control precise neural codes. For soCoChR-GFP-expressing neurons we demonstrate that APs can be generated reliably by using either a conventional mode-locked femtosecond Ti:sapphire laser or an amplified fiber laser. The first approach is easier to implement, since such laser sources are common in 2P microscopy. However, we found that reaching the AP threshold with soCoChR at a depth of about 50 μm required an excitation power of about 30 mW/cell. This value, considering an available exit power after the objective of ~200 mW (at 920 nm), will limit the maximum number of simultaneously achievable targets to six or seven cells. Amplified fiber lasers enable higher 2P absorption compared to typical mode-locked Ti:sapphire laser oscillators due to

lower pulse repetition rates of the femtosecond laser (the 2P excited signal $S \propto P_{avg}^2 \left(f t_p \right)^{-1}$, with f the repetition rate, t_p the pulse width and P_{avg} the average beam power[41]). This feature enabled reducing to ~80 µW/µm² (corresponding to about 9 mW/cell) the AP spiking threshold and therefore, considering the several-watt exit power of amplified fiber lasers (corresponding in our setup to ~2 W after the objective), would make it possible to simultaneously photostimulate up to 200 cells. Performances similar to the one achieved with targeted CoChR and 2P holographic illumination might be reached by other opsins when fused to the KA2(1–150) motif; for example, Jaws could be used for neuronal inhibition[42].

Single-cell optogenetics may prove powerful for mapping the connectivity of neurons within functional networks, a topic of great interest in the understanding of how individual cells work together in networks to implement neural computation. Past attempts to map connectivity, either by multi-neuron simultaneous whole-cell patch clamp[43], by glutamate uncaging onto populations of cells[44], by examining spontaneous activity in neural networks[45] or by laser-scanning photoactivation of populations of neurons equipped with optogenetic actuators[46], have revealed many tantalizing and nonrandom features of mammalian neural circuits, with consequences for understanding how individual neurons and networks compute, generate behavior and contribute to brain pathology. With zero-spike crosstalk single-cell optogenetics, it will be possible to patch one neuron and photostimulate many neighboring cells, measuring synaptic strength as well as synaptic release kinetics, and perhaps also to image neural activity network-wide in response to each neuron within the network being excited in turn. Thus, the technologies we report here will be useful for bridging the structural and functional domains of the field of connectomics, important for ultimately realizing its impact on the understanding of behavior and disease.

Methods

Methods, including statements of data availability and any associated accession codes and references, are available at https://doi.org/10.1038/s41593-017-0018-8.

References

1. Boyden, E. S. A history of optogenetics: the development of tools for controlling brain circuits with light. *F1000 Biol. Repc.* **3**, 11 (2011).
2. Dombeck, D. A., Harvey, C. D., Tian, L., Looger, L. L. & Tank, D. W. Functional imaging of hippocampal place cells at cellular resolution during virtual navigation. *Nat. Neurosci.* **13**, 1433–1440 (2010).
3. Li, C.-Y. T., Poo, M.-M. & Dan, Y. Burst spiking of a single cortical neuron modifies global brain state. *Science* **324**, 643–646 (2009).
4. Houweling, A. R. & Brecht, M. Behavioural report of single neuron stimulation in somatosensory cortex. *Nature* **451**, 65–68 (2008).
5. Rickgauer, J. P. & Tank, D. W. Two-photon excitation of channelrhodopsin-2 at saturation. *Proc. Natl. Acad. Sci. USA* **106**, 15025–15030 (2009).
6. Ronzitti, E. et al. Recent advances in patterned photostimulation for optogenetics, *J. Opt.* **19**, 113001 (2017).
7. Papagiakoumou, E. et al. Scanless two-photon excitation of channelrhodopsin-2. *Nat. Methods* **7**, 848–854 (2010).
8. Papagiakoumou, E., de Sars, V., Oron, D. & Emiliani, V. Patterned two-photon illumination by spatiotemporal shaping of ultrashort pulses. *Opt. Express* **16**, 22039–22047 (2008).
9. Bègue, A. et al. Two-photon excitation in scattering media by spatiotemporally shaped beams and their application in optogenetic stimulation. *Biomed. Opt. Express* **4**, 2869–2879 (2013).
10. Chaigneau, E. et al. Two-photon holographic stimulation of ReaChR. *Front. Cell. Neurosci.* **10**, 234 (2016).
11. Ronzitti, E. et al. Sub-millisecond optogenetic control of neuronal firing with two-photon holographic photoactivation of Chronos. *J. Neurosci.* https://doi.org/10.1523/JNEUROSCI.1246-17.2017 (2017).
12. Hernandez, O. et al. Three-dimensional spatiotemporal focusing of holographic patterns. *Nat. Commun.* **7**, 11928 (2016).
13. Papagiakoumou, E. et al. Functional patterned multiphoton excitation deep inside scattering tissue. *Nat. Photonics* **7**, 274–278 (2013).
14. Packer, A. M. et al. Two-photon optogenetics of dendritic spines and neural circuits. *Nat. Methods* **9**, 1202–1205 (2012).
15. Anselmi, F., Ventalon, C., Bègue, A., Ogden, D. & Emiliani, V. Three-dimensional imaging and photostimulation by remote-focusing and holographic light patterning. *Proc. Natl. Acad. Sci. USA* **108**, 19504–19509 (2011).
16. Dal Maschio, M., Donovan, J. C., Helmbrecht, T. O. & Baier, H. Linking neurons to network function and behavior by two-photon holographic optogenetics and volumetric imaging. *Neuron* **94**, 774–789.e5 (2017).
17. Nicholson, C. & Syková, E. Extracellular space structure revealed by diffusion analysis. *Trends Neurosci.* **21**, 207–215 (1998).
18. Valluru, L. et al. Ligand binding is a critical requirement for plasma membrane expression of heteromeric kainate receptors. *J. Biol. Chem.* **280**, 6085–6093 (2005).
19. Klapoetke, N. C. et al. Independent optical excitation of distinct neural populations. *Nat. Methods* **11**, 338–346 (2014).
20. Jacobs, E. C., Bongarzone, E. R., Campagnoni, C. W., Kampf, K. & Campagnoni, A. T. Soma-restricted products of the myelin proteolipid gene are expressed primarily in neurons in the developing mouse nervous system. *Dev. Neurosci.* **25**, 96–104 (2003).
21. Lim, S. T., Antonucci, D. E., Scannevin, R. H. & Trimmer, J. S. A novel targeting signal for proximal clustering of the Kv2.1 K+ channel in hippocampal neurons. *Neuron* **25**, 385–397 (2000).
22. Garrido, J. J. et al. A targeting motif involved in sodium channel clustering at the axonal initial segment. *Science* **300**, 2091–2094 (2003).
23. Schäfer, M. K. E. et al. L1 syndrome mutations impair neuronal L1 function at different levels by divergent mechanisms. *Neurobiol. Dis.* **40**, 222–237 (2010).
24. Bianco, A., Dienstbier, M., Salter, H. K., Gatto, G. & Bullock, S. L. Bicaudal-D regulates fragile X mental retardation protein levels, motility, and function during neuronal morphogenesis. *Curr. Biol.* **20**, 1487–1492 (2010).
25. Ran, B., Bopp, R. & Suter, B. Null alleles reveal novel requirements for Bic-D during *Drosophila* oogenesis and zygotic development. *Development* **120**, 1233–1242 (1994).
26. Zhang, X. & Bennett, V. Restriction of 480/270-kD ankyrin G to axon proximal segments requires multiple ankyrin G-specific domains. *J. Cell Biol.* **142**, 1571–1581 (1998).
27. Wu, C., Ivanova, E., Zhang, Y. & Pan, Z.-H. rAAV-mediated subcellular targeting of optogenetic tools in retinal ganglion cells in vivo. *PLoS One* **8**, e66332 (2013).
28. Greenberg, K. P., Pham, A. & Werblin, F. S. Differential targeting of optical neuromodulators to ganglion cell soma and dendrites allows dynamic control of center-surround antagonism. *Neuron* **69**, 713–720 (2011).
29. Marchler-Bauer, A. et al. CDD: NCBI's conserved domain database. *Nucleic Acids Res.* **43**, D222–D226 (2015).
30. Ren, Z. et al. Multiple trafficking signals regulate kainate receptor KA2 subunit surface expression. *J. Neurosci.* **23**, 6608–6616 (2003).
31. Grubb, M. S. & Burrone, J. Channelrhodopsin-2 localised to the axon initial segment. *PLoS One* **5**, e13761 (2010).
32. Zhang, Z., Feng, J., Wu, C., Lu, Q. & Pan, Z.-H. Targeted expression of channelrhodopsin-2 to the axon initial segment alters the temporal firing properties of retinal ganglion cells. *PLoS One* **10**, e0142052 (2015).
33. Baker, C. A., Elyada, Y. M., Parra, A. & Bolton, M. M. Cellular resolution circuit mapping with temporal-focused excitation of soma-targeted channelrhodopsin. *Elife* **5**, e14193 (2016).
34. Helmchen, F. & Denk, W. Deep tissue two-photon microscopy. *Nat. Methods* **2**, 932–940 (2005).
35. Szabo, V., Ventalon, C., De Sars, V., Bradley, J. & Emiliani, V. Spatially selective holographic photoactivation and functional fluorescence imaging in freely behaving mice with a fiberscope. *Neuron* **84**, 1157–1169 (2014).
36. Brill, J., Mattis, J., Deisseroth, K. & Huguenard, J. R. LSPS/optogenetics to improve synaptic connectivity mapping: unmasking the role of basket cell-mediated feedforward inhibition. *eNeuro* **3**, ENEURO.0142–15.2016 (2016).
37. Kohara, K. et al. Cell type-specific genetic and optogenetic tools reveal hippocampal CA2 circuits. *Nat. Neurosci.* **17**, 269–279 (2014).
38. Little, J. P. & Carter, A. G. Subcellular synaptic connectivity of layer 2 pyramidal neurons in the medial prefrontal cortex. *J. Neurosci.* **32**, 12808–12819 (2012).
39. Pala, A. & Petersen, C. C. In vivo measurement of cell-type-specific synaptic connectivity and synaptic transmission in layer 2/3 mouse barrel cortex. *Neuron* **85**, 68–75 (2015).
40. Liu, X. et al. Optogenetic stimulation of a hippocampal engram activates fear memory recall. *Nature* **484**, 381–385 (2012).
41. Xu, C. & Webb, W. W. Measurement of two-photon excitation cross sections of molecular fluorophores with data from 690 to 1050 nm. *J. Opt. Soc. Am. B* **13**, 481 (1996).
42. Chuong, A. S. et al. Noninvasive optical inhibition with a red-shifted microbial rhodopsin. *Nat. Neurosci.* **17**, 1123–1129 (2014).

43. Song, S., Sjöström, P. J., Reigl, M., Nelson, S. & Chklovskii, D. B. Highly nonrandom features of synaptic connectivity in local cortical circuits. *PLoS Biol.* **3**, e68 (2005).
44. Yoshimura, Y., Dantzker, J. L. M. & Callaway, E. M. Excitatory cortical neurons form fine-scale functional networks. *Nature* **433**, 868–873 (2005).
45. Ikegaya, Y. et al. Synfire chains and cortical songs: temporal modules of cortical activity. *Science* **304**, 559–564 (2004).
46. Petreanu, L., Huber, D., Sobczyk, A. & Svoboda, K. Channelrhodopsin-2-assisted circuit mapping of long-range callosal projections. *Nat. Neurosci.* **10**, 663–668 (2007).

Author contributions

O.A.S. designed, screened and tested soma-targeted opsins. O.A.S., C.L. and K.P. performed and analyzed 1P experiments in cultured cells. V.Z. and D.T. performed and analyzed 2P experiments in cultured cells and brain slices. V.Z. performed and optimized virus injection and implemented electrophysiological recording on the 2P rigs. E.R. and E.P. designed and built up setup 1. D.T. designed and built up setup 2, optimized multicell stimulation and designed calibration procedures. O.A.S., E.S.B., D.T., V.Z. and V.E. interpreted data, designed experiments, and wrote the paper with contributions from all authors. E.S.B. and V.E. conceived and supervised the project.

Competing interests

O.A.S., E.S.B. and C.L. are inventors on pending patents covering the described work.

Additional information

Supplementary information is available for this paper at https://doi.org/10.1038/s41593-017-0018-8.

Reprints and permissions information is available at www.nature.com/reprints.

Correspondence and requests for materials should be addressed to E.S.B. or V.E.

Publisher's note: Springer Nature remains neutral with regard to jurisdictional claims in published maps and institutional affiliations.

Methods

Primary neuron culture, transfection and transduction. All procedures involving animals were in accordance with the National Institutes of Health *Guide for the Care and Use of Laboratory Animals* and approved by the Massachusetts Institute of Technology Animal Care and Use Committee. Hippocampal neuron cultures were prepared from postnatal day 0 or day 1 Swiss Webster (Taconic or Charles River) mice as previously described[19].

For neuronal expression of GFP fusions with opsins or GFP fusions with trafficking sequences during the screen for soma targeting sequences, we performed transfection at 4 days in vitro (DIV) with a commercial calcium phosphate kit (Invitrogen). We added an additional washing step with acidic MEM buffer (pH 6.8–6.9) after calcium phosphate precipitate incubation to completely resuspend residual precipitates[47]. We used 1 μg of DNA. Neurons were imaged 14–18 DIV (10–14 d after transfection).

For neuronal expression of mCherry we transduced the already transfected neurons at 10–14 DIV with AAV8-Syn-mCherry-WPRE virus by adding 1 μl of the virus (titer 1.4×10^{13} infectious units per mL).

For neuronal expression of either CoChR-GFP or soCoChR-GFP in culture (as seen in Fig. 2), hippocampal cultures were transduced at 3–4 DIV with either AAV8-Syn-CoChR-GFP-WPRE or AAV8-Syn-soCoChR-GFP-WPRE viruses (at a titer of 4.7×10^{12} and 4.0×10^{12}, respectively) and imaged 14 d later.

AAV particles were produced by the University of North Carolina Chapel Hill Vector Core.

Whole-cell electrophysiology in vitro. *Current and voltage clamp recordings of cultured neurons.* Whole cell patch clamp recordings in culture were made using Axopatch 200B or Multiclamp 700B amplifiers, a Digidata 1440 digitizer and a PC running pClamp (Molecular Devices). For in vitro current-clamp recordings, neurons were patched at 14–18 DIV (10–14 d after transfection) to allow neurons to mature to the point of being capable of spiking. Neurons were bathed in room temperature Tyrode buffer containing 125 mM NaCl, 2 mM KCl, 3 mM CaCl$_2$, 1 mM MgCl$_2$, 10 mM HEPES, 30 mM glucose and the receptor blockers 0.01 mM NBQX and 0.01 mM gabazine. The Tyrode pH was adjusted to 7.3 with NaOH and the osmolarity was adjusted to 300 mOsm with sucrose. For in vitro voltage-clamp recordings, neurons were patched at 19–21 DIV (17–20 d after transfection) under similar conditions as for the current-clamp recordings, except the Tyrode also contained 1 μM tetrodotoxin (Tocris Bioscience). No all-*trans*-retinal was added for any cultured neuron recordings.

For recordings, borosilicate glass pipettes (Warner Instruments) with an outer diameter of 1.2 mm and a wall thickness of 0.255 mm were pulled to a resistance of 5–10 MΩ with a P-97 Flaming/Brown micropipette puller (Sutter Instruments) and filled with a solution containing 125 mM potassium gluconate, 8 mM NaCl, 0.1 mM CaCl$_2$, 0.6 mM MgCl$_2$, 1 mM EGTA, 10 mM HEPES, 4 mM Mg-ATP and 0.4 mM Na-GTP. The pipette solution pH was adjusted to 7.3 with KOH and the osmolarity was adjusted to 298 mOsm with sucrose. For voltage clamp experiments, cells were clamped at −65 mV. For current clamp experiments, access resistance was monitored throughout recording. Data were analyzed using Clampfit (Molecular Devices) and custom Matlab scripts (MathWorks, Inc.).

Current clamp recordings of cultured neurons during digital micromirror device (DMD) photostimulation experiments. Whole-cell patch clamp recordings were made using Axopatch 200B or Multiclamp 700B amplifiers, a Digidata 1440 digitizer and a PC running pClamp (Molecular Devices). In each experiment (Fig. 2), we patched (current clamp) cell 1. Then, starting from cell 1, we photostimulated cell 1 and 9 other cells using the DMD to focus the light. Photostimulations were made 10 s apart (470 nm; 40.7 mW/mm^2) and the responses for the photostimulation were recorded in pClamp.

Molecular cloning and virus production. All opsin genes were synthesized (Genscript) with mammalian codon optimization and subcloned as previously described[19,48]. For screening in cultured neurons, all genes were subcloned into the FCK lentiviral backbone under a CaMKII promoter (derived from the promoter from the gene *Camk2a*) and with a C-terminal GFP fusion. For soCoChR-GFP, the first 450 bp were cloned 3′ to CoChR, with no further trafficking sequences added. For CoChR-Na$_v$1.2(II–III)-GFP, we added the KGC[49] followed by ER2[50] trafficking sequences from the potassium channel Kir2.1, with the resulting molecule named CoChR-KGC-Na$_v$1.2(II–III)-ER2-GFP (see ref. [42] for earlier details). For virus production, the genes were cloned into the pAAV plasmid, using a synapsin promoter. AAV (serotype 8) was produced by the UNC vector core.

Photostimulation experiments in vitro. *Whole field neural stimulation.* Neuron voltage clamp photostimulation experiments were done with a LED mounted on a microscope for widefield illumination (Leica 3000B), with a nominal wavelength of 480 nm (X-Cite XLED1, Excelitas Technologies). We filtered the LED light with the 472/30 nm BrightLine single-band bandpass filter (Semrock). Light was triggered by pClamp (Molecular Devices). Light power was measured as 34.84 mW/mm^2 through a Leica HCX APO L 40× objective (air, NA 0.6). For each trace recorded, a 10-ms current injection was given (to make sure a neuron could spike), followed by a 1-ms light pulse (480 nm; 34.84 mW/mm^2) 5 s later.

Stimulation of cell bodies with a DMD. Stimulation of neural cell bodies was performed with a Leica 6000 B widefield microscope mounted with a Mosaic DMD system (Andor) and a Zyla 5.5 sCMOS camera (Andor). The experiments were performed with an LED with a nominal wavelength of 470 nm (Thorlabs, M470L2) and power of 40.7 mW/mm^2. Neurons were imaged and stimulated through a 1 MP-2262-59022XR-360T GFP/mCherry filter set (dual GFP/mCherry, Andor). For the photostimulation experiment, an image of the green fluorescence was first acquired, and cell bodies were then identified by eye on the basis of their doughnut-shaped fluorescence. A cell was chosen at random to be patched (to avoid sample bias, we patched the neuron that was closest to the middle of the field of view), with the only requirement being that it was in a dense area. This cell was referred to as cell 1. Thereafter, 9 circles with a diameter of 20 μm were defined around cell bodies of interest using MetaMorph software (Molecular Devices) with distances ranging between 10 and 200 μm from cell 1. Then, starting from cell 1, we photostimulated cell 1 and the 9 other cells sequentially. Stimulations were made 10 s apart.

Single-photon characterization of CoChR and soCoChR. Action spectrum data for CoChR and soCoChR were taken and analyzed as previously described[19]. Analysis of spike probability as a function of irradiance for CoChR- and soCoChR-expressing cells, photocurrent as a function of irradiance for CoChR- and soCoChR-expressing cells, and light-driven spike fidelity for CoChR- and soCoChR-expressing cells were all determined as previously described[19].

Imaging in vitro. GFP fusions with trafficking sequences, opsin-GFP with trafficking sequences, and cytosolic mCherry expressed in cultured neurons were imaged with a LED (X-Cite XLED1, Excelitas Technologies) mounted on a microscope for widefield illumination (Leica 3000B) through either a Leica HCX APO L 40× objective (air, NA 0.6) or a Leica HCX APO L 20× objective (air, NA = 0.5). Imaging was performed with a Hamamatsu Orca Flash 4.0 camera under identical illumination conditions throughout: a 480-nm LED using a GFP-3035D filter cube (Semrock) for GFP fluorescence (34.84 mW/mm^2) and a 540-nm LED with a 543 nm ± 11 nm excitation filter (Semrock) for mCherry fluorescence. Images were taken with an exposure time of 300 ms.

Cultured neurons expressing CoChR-GFP, KA2-GFP or KA2(1–150)-GFP were imaged using similar parameters: fluorescence was excited with a 480 nm LED filtered by a 472/30 nm BrightLine single-band bandpass filter (Semrock) and focused on the sample through a Leica HCX APO L 20× objective (air, NA 0.6), with a power of 25.19 mW/mm^2. Images were acquired with a Hamamatsu Orca Flash 4.0 with an exposure time of 300 ms.

Viral injections and whole-cell electrophysiology in brain slices. All experimental procedures were conducted in accordance with guidelines from the European Union and institutional guidelines on the care and use of laboratory animals (council directive 86/609 of the European Economic Community) that were approved by the Paris Descartes Ethics Committee for Animal Research (registration number CEEA34.EV.118.12).

Stereotactic injections of the viral vectors AAV8-Syn-CoChR-GFP, AAV8-Syn -CoChR-KGC-Na$_v$1.2(II–III)-GFP-ER2 and AAV8-Syn-soCoChR-GFP were performed in 4-week-old male Swiss mice (Janvier Labs). For connectivity experiments the promoters Syn (derived from the human *SYN1* promoter), CaMKII (derived from the promoter from *Camk2a*) or CAG were used. Animals were housed from 3 to 5 per cage with a light dark cycle of 12 + 12 h. Mice were anesthetized with a ketamine (80 mg/kg)–xylazine (5 mg/kg) solution and a small craniotomy (0.7 mm) was made on the skull overlying V1 cortex. An injection of 1–1.5 μl solution containing the viral vector was made with a cannula at about 80–100 nl/min at 200–250 μm below the dural surface. The skin was sutured and the mouse recovered from anesthesia.

Brain slices of V1 cortex were prepared from mice 7–15 weeks after viral injection. Mice were deeply anesthetized with isoflurane (5% in air) and decapitated, and the brain was rapidly removed. Sagittal slices 300 μm thick were obtained (VT1200S Leica Biosystems, Germany) in room temperature or ice-cold solution containing the following (in mM): 85 NaCl, 2.5 KCl, 0.5 CaCl$_2$, 4 MgCl$_2$, 65 sucrose, 25 glucose, 0.5 ascorbic acid. Slices were transferred to a recovery chamber held at 35° for 45 min, in a bath containing 20% sucrose solution and 80% ACSF containing the following (in mM): 125 NaCl, 2.5 KCl, 26 NaHCO$_3$, 1.25 NaH$_2$PO$_4$, 1 MgCl$_2$, 1.5 CaCl$_2$, 25 glucose, 0.5 ascorbic acid. All solutions were aerated with 95% O$_2$ and 5% CO$_2$ to a final pH of 7.4.

Slices were placed in a recording chamber under the microscope objective and were patched while monitoring IR transmitted light images acquired at approximately video rate. Cells were patched at 40–70 μm depth and clamped at −70 mV in voltage-clamp configuration. Membrane potential was kept at −70 mV with current injections ranging from −5 to −35 pA in current-clamp configuration. Cell type was established on the basis of morphology and AP firing properties. Electrophysiology data were acquired with a Multiclamp 700B amplifier, a Digidata 1322 A digitizer (Molecular Devices) or a National Instrument device, and a PC running pClamp10 software (Molecular Devices) or Neuromatic software running on the IgorPro interface (Wavemetrics). Voltage and current clamp recordings were filtered at 6–10 kHz and sampled at 20–50 kHz. On the curves displayed in

Fig. 3, a smoothing of between 150 and 250 data points was applied, and in Fig. 5 a smoothing of 10 data points was applied.

The following receptor blockers were added to the artificial cerebrospinal fluid (ACSF) solution in all experiments to block any synaptic effect: strychnine, picrotoxin, gabazine and NBQX (1–5 µM each; from Abcam or Tocris). Borosilicate glass pipettes (outer diameter 1.5 mm and inner diameter 0.86 mm) were pulled with a micropipette puller (Sutter Instruments) and filled with a solution containing the following (in mM): 130 potassium gluconate, 7 KCl, 4 Mg-ATP, 0.3 mM Na-GTP, 10 sodium phosphocreatine and 10 mM HEPES (pH adjusted to 7.28 with KOH; osmolarity 280 mOsm). Pipette resistance in the bath was 5–7 MΩ. Data were acquired with a Multiclamp 700B amplifier, a Digidata 1322 A digitizer (Molecular Devices) or a National Instrument device, and a PC running pClamp10 software (Molecular Devices) or Neuromatic software running on the IgorPro interface (Wavemetrics).

Imaging and photostimulation in brain slices. Holographic photostimulation was implemented in two different setups, with two different photostimulation laser sources and imaging systems. Setups 1 and 2 were used to acquire the data presented in Figs. 3, 4 and 6 whereas data presented in Fig. 5 were acquired solely with setup 1.

Setup 1. Setup 1 consists of a homemade system, built around a commercial upright microscope (SliceScope, Scientifica) in which the holographic photostimulation path was combined with three imaging pathways: a two-photon (2P) raster-scanning pathway, a one-photon (1P) widefield epifluorescence pathway and an infrared (IR) transmitted-light imaging pathway (see schematic in Supplementary Fig. 6). 2P imaging was performed with a pulsed Ti:sapphire laser source (Coherent Chameleon Vision II, pulse width 140 fs, tuning range 680–1,080 nm). The beam was raster scanned across the sample via a pair of xy galvanometric mirrors (3-mm aperture, 6215 H series, Cambridge Technology) imaged at the back aperture of the microscope objective (40× W APO NIR, Nikon) through an afocal telescope (scan lens: $f = 100$ mm, Thorlabs AC508-300-B; tube lens: $f = 300$ mm, Thorlabs AC508-100-B). Fluorescence was collected with a fiber-coupled detection scheme[51] based on a large-diameter collector lens ($f = 75$ mm, Thorlabs LB1309-A) and a 5-mm-diameter liquid light guide (LLG, Series 300, Lumatec customized with a $f = 14.5$ mm doublet lens glued at the fiber entrance, by Till Photonics, and an anti-reflective coating provided at the fiber exit). The exit of the fiber was projected onto two GaAsP photomultiplier tubes (H10770-40 SEL, Hamamatsu H10770-40 SEL, active area 5 mm) by a set of three matching aspheric lenses ($f = 23.5$ mm, Melles Griot LAG-32.5-23.5-C). Fluorescence light was filtered by an IR-blocking filter (FF01-750sp, Semrock), spectrally split into two channels by a dichroic mirror (FF555-Di03, Semrock) and further filtered through two emission filters (FF01-510/84 and FF02-617/73, Semrock). The power of the 2P imaging laser was controlled through a liquid crystal variable phase retarder (LRC-200-IR1, Meadowlark Optics) and a polarizer cube (BB-050-IR1, Meadowlark Optics).

1P imaging was based on illumination provided by a LED source (M470L2, Thorlabs), whose emission spectra was filtered by a bandwidth excitation filter (FF01-452/45, Semrock). To provide homogenous widefield illumination, the emission was directed though a diffuser (DG10-1500, Thorlabs) and successively through an achromatic lens ($f = 30$ mm, LA1805 Thorlabs). 1P-induced fluorescence, after being separated from the excitation light using a dichroic mirror (FF510-Di02, Semrock), was collected through a tube lens ($f = 200$ mm), filtered by a band-pass filter (FF01-609/181, Semrock) and detected by a CCD camera (Orca-05G, Hamamatsu). Fluorescence induced by 2P raster scanning or by 1P widefield illumination was collected by PMTs or a CCD, respectively; in the detection pathway we had a switchable dichroic mirror (FF705-Di01, 70 × 50 mm custom size, Semrock).

The transmitted IR oblique illumination imaging path was based on an IR LED source (M780L2, Thorlabs), coupled with a DODT-contrast tube (DODT tube, Scientifica) and a condenser. Light transmitted through the sample was collected with an IR CCD (IR-1000, DAGE-MIT).

2P photoactivation consisted of arbitrary illumination patterns obtained with computer-generated holography, based on phase modulation of the laser wave front via the use of a spatial light modulator (SLM).

The laser source used consisted of a femtosecond pulsed beam delivered by a fiber laser source (pulse width 250 fs, repetition rate 500 kHz, pulse energy 20 µJ, $\lambda = 1,030$ nm; Satsuma, Amplitude Systems). The beam was enlarged by a telescope and reflected off the SLM (LCOS-SLM X10468-07, Hamamatsu Photonics). The beam was then projected on the back focal plane of the objective with a double afocal telescope ($f = 500$ mm Thorlabs AC508-500-B, $f = 300$ mm, Thorlabs AC508-300-B, $f = 200$ mm, Thorlabs AC508-200-B and $f = 300$ mm Thorlabs AC508-300-B). The SLM was driven by custom-designed software (Wave Front Designer[52]) based on a Gerchberg and Saxton (GS) iterative algorithm[53] that converts an arbitrary intensity pattern on the sample plane to a specific phase profile to be addressed at the SLM plane.

As originally described for low-NA[54] and, more recently, high-NA objectives[12], adding lens-phase modulations to 2D-phase holograms enables remote axial displacement and 3D positioning of bidimensional light patterns. This allowed us to target neural processes, following their path in x-y-z (Fig. 3), and to address multiple targets, sequentially or simultaneously, on multiple planes (Figs. 5 and 6).

The zeroth order of diffraction was eliminated by introducing a single or a double cylindrical lens[55]. 2P imaging scanning and 2P photoactivation beams were combined through a large dichroic mirror (Chroma T970dcspxr, 50 mm × 70 mm custom size, Chroma).

Setup 2. An analogous holographic photostimulation path was coupled with widefield epifluorescence imaging on a second system, here denoted as setup 2 (see Supplementary Fig. 6). This system was built around an Olympus BX51WI upright microscope, capable of widefield epifluorescence imaging using illumination with an arc lamp (OptoSource Illuminator, Cairn Research, coupled with a monochromator, Optoscan Monochromator, Cairn Research), and an Orca Flash 4.0 Hamamatsu sCMOS camera for epifluorescence imaging. The native infrared differential interference contrast (DIC) path of the Olympus microscope allowed DIC imaging on the camera. The holographic photoactivation laser source consisted of a conventional pulsed Ti:sapphire laser used at 920 nm (pulse width: 100 fs, repetition rate: 80 MHz, Mai-Tai, Deep-See, Spectra Physics).

The holographic path was analogous to the one described for setup 1: a beam expander enlarged the beam in front of the spatial light modulator (LCOS-SLM X10468-02), whose plane was projected at the back focal plane of a 40×, NA 0.8 objective (LUM PLAN FI/IR, Olympus) by an afocal telescope ($f = 750$ mm, Thorlabs AC508-750-B and $f = 500$ mm Thorlabs AC508-500-B). The holographic beam was coupled to the optical axis of the microscope by a dichroic mirror (FF670, SDi01, 25 × 36 mm, Semrock). Photostimulation light pulses were generated by a Pockels cell (350-80, Conoptics). For the experiments in Fig. 6, setup 2 was upgraded with a commercial 2P scanning imaging module (VIVO, 2-PHOTON, 3i-Intelligent Imaging Innovations).

Power conversion between setups 1 and 2. The differences between the illumination conditions (wavelength, pulse width and repetition rate) used in setups 1 and 2 required finding a proper criterion to compare the experiments performed on the two setups. To do so, we empirically estimated a scaling conversion factor k between the power of the two systems, P_1 on setup 1 and P_2 on setup 2, based on measurements of the rise times (τ_{on}) of photo-induced currents (see Fig. 4): we take as the conversion factor k the ratio between the powers that in each setup induced a photocurrent with the same rise time. We fit the dependence of the rise times on the excitation power ($n = 4$ cells measured in setup 1, among which 3 expressed CoChR-GFP and 1 soCoChR-GFP; $n = 5$ cells measured on setup 2, among which 2 expressed CoChR-GFP and 3 soCoChR-GFP), using the expression

$$\tau_{on,i}(P_i) = \frac{c_1}{(P_i + c_2)^2} + c_3 \tag{1}$$

where P_i is the photostimulation power density (with $i = 1$ or 2 indicating setup 1 or setup 2, respectively) and c_1, c_2 and c_3 are three free fitting parameters. For each cell, the experimental dependence of the rise time on the illumination power included at least five power values.

The conversion factor $k = P_2/P_1$ was obtained as the factor that minimized the mean square difference between the values of the curve $\tau_{on,1}(P_1)$ and those of the curve with the rescaled power values $\tau_{on,2}(kP_1)$. The value thus obtained was $k = P_2/P_1 \approx 5.3$, meaning that powers used in setup 1 were about one-fifth those used in setup 2.

Diffraction efficiency corrections. Holographically generated light patterns suffer from a position-dependent diffraction efficiency[12,56,57], meaning that the intensity of a holographic spot decreases with distance from the center of the field of view or from the nominal focal plane of the objective. Therefore, generation of illumination patterns with uniform intensity, crucial for the experiments in Figs. 3, 5 and 6, required the implementation of corrective algorithms to compensate for this effect.

In the case of sequential targeting of different locations, homogenization of light distribution was achieved by generating, together with the excitation holographic spots of surface A_{spot}, an additional correction spot at the edge of the field of view, of surface A_{corr}. By adjusting the size of the correction spot we could modulate the light intensity in the excitation spot while moving the latter across the excitation field, thus achieving constant light illumination (see Supplementary Fig. 11). More precisely, at first we characterized experimentally the position-dependent diffraction efficiency, DE(x, y, z); then, given a sequence of N illumination spots of coordinates (x_i, y_i, z_i), we set the surface of the correction spot for each illumination site to be

$$A_{corr_i} = A_{spot} \cdot \left(\frac{DE(x_i, y_i, z_i)}{\min_N DE} - 1 \right)$$

where $\min_N$ DE is the lowest diffraction efficiency value over the N illumination sites. The correction spot was blocked at an intermediate image plane after the spatial light modulator, preventing it from reaching the sample.

For simultaneous illumination of multiple spots we used, as described by Conti et al.[58] and Hernandez et al.[12], graded input patterns to calculate with the iterative GS algorithm the corresponding phase mask (see Supplementary Fig. 11). Briefly,

each illumination spot, the ith in the ensemble of N, drawn in the input image for the GS algorithm was weighted with a subunitary coefficient w_i, given by

$$w_i = \frac{\min_N DE}{DE(x_i, y_i, z_i)}$$

This enabled us to direct more power to spots corresponding to regions with low diffraction efficiency while sending less power to the spots closer to the center of the excitation field and/or the objective focal plane.

Finally, we equalized the excitation power densities used for single-spot sequential stimulation and simultaneous multiple spot stimulation by adjusting the exit laser power.

Holographic photostimulation along neurites. Patched cells in slices were loaded with Alexa 594 hydrazide dye (15–20 μM; Invitrogen) to visualize cell morphology. We imaged the patched neuron loaded with Alexa 594 with a 2P scanning imaging system (imaging laser at 780 nm, setup 1)[59] or widefield illumination (at 570 nm, setup 2). A z-stack of the fluorescence emission was acquired to reconstruct the 3D morphology of the neurites (in a range of typically ± 40 μm) and to target, with holographic illumination, specific x-y-z positions along neurites.

The photostimulation protocol consisted of sequentially displacing 10-μm-diameter holographic stimulation spots from the distal end of the process toward the soma, with a step size of approximately 10 μm. 2P stimulation consisted of 30-ms pulses with an illumination power density corresponding to the power threshold density required to trigger one AP when stimulating the whole soma. Practically, the power threshold density was obtained by progressively increasing the excitation power up to a value that allowed us to reliably (in three consecutive trials) trigger one AP each time.

Measurement of opsin and photo-induced AP kinetic parameters. Neurons expressing CoChR-GFP or soCoChR-GFP were patched and photostimulated with holographic spots whose diameter was between 10 and 15 μm—i.e., covering the whole soma. The kinetics of the response was monitored in both current-clamp and voltage-clamp configurations. The photostimulation consisted of pulses of holographic illumination with a duration varying from 300 ms at low power down to a few milliseconds at high power. The reported rise time τ_{on} corresponds to the time constant of a monoexponential fit of the ascending part of the photo-induced current.

To estimate the asymptotic value of the rise time, we fit the rise time vs. power curve of each cell with equation (1). The coefficient c_3 was taken as the asymptotic value of the rise time for each cell and then averaged across cells. We considered in the average only cells in which the rise time vs. power curve had a sufficient number of experimental points (≥ 5) to assure the reliability of the fit.

The AP latency was defined as the time delay between the onset of 2P stimulation and the peak of the photostimulated AP. The plotted values were obtained by averaging AP latencies across 5 photostimulations (separated by 30 s). The duration of the photostimulation pulse was initially set to 30 ms for low stimulation power (22 ± 19 μW/μm²). For high photostimulation power (107 ± 29 μW/μm²), we decreased the duration of photostimulation to <30 ms to minimize the generation of multiple spikes. The reported jitter was calculated as the s.d. of the AP latency computed across 5 consequent photostimulations. The values were extracted from the same data used to obtain the latency values.

Multiple-cell-soma holographic photostimulation in slices. Opsin-expressing cells were visualized with a 2P scanning imaging system (imaging laser at $\lambda = 920$ nm in setup 1) and patched. Thereafter, a z-stack of the GFP fluorescence emission in the volume around the patched cell was acquired to identify neighboring positive cells. The scanning imaging lasers, although inducing some photocurrents ($I = 23 \pm 13$ pA; imaging power $P = 14 \pm 2$ mW, scanning frequency 0.74 Hz; $n = 3$ soCoChR-expressing cells from 3 mice), did not induce APs during imaging. In slices expressing soCoChR-GFP, cells were clearly distinguishable, since predominantly their somata were fluorescent, with minimal neuropil fluorescence. In contrast, slices expressing CoChR-GFP presented a diffuse and homogeneous green fluorescence, in which cells could be recognizable as dark spots (spots with lower fluorescence than background).

In the volume around the patched cells, we randomly identified and selected an ensemble of neighboring fluorescent cells that we targeted with 10–14 μm holographic spots. Depending on the field of view and cell distribution, we selected 5 to 8 cells. To avoid broadening of axial resolution due to the axial overlapping of multiple spots, for cells separated by an axial distance smaller than the spot FWHM (see Supplementary Fig. 8) we chose cells that were laterally shifted with respect to one another. These cells, in the vicinity of the patched cell, were sequentially stimulated with a holographic spot (30-ms illuminations, 5 s apart) and the generated membrane depolarizations recorded. The last cell to be photostimulated for each stimulation sequence was the patched cell. Receptor blockers were added to the ACSF solution in all experiments to block any synaptic effects (strychnine, picrotoxin, gabazine and NBQX, 1–5 μM; Abcam or Tocris).

For sequential and simultaneous illumination experiments, the same power density was delivered to each spot in the pattern, thanks to our diffraction efficiency

compensating algorithm (see above). Since the axial separation between the patched cell and targeted neighboring cells was <30 μm, we estimated[60] that the effects of scattering on the relative intensity between spots on the patched soma and on neighboring cells were less than 10% and were therefore negligible. For higher spatial separations, a uniform light distribution was obtained by adding further corrections to the intensity of each illumination spot according to axial position.

3D holographic pattern reconstruction and calibration. To reconstruct the 3D holographic illumination pattern in Fig. 5b and Supplementary Figs. 8 and 11, we used a dual microscope configuration as previously described[8,9,12,52]. Briefly, below the main upper objective we placed a second objective (NA 1.2, water immersion, 60×). While the upper objective focused the holographic pattern on a thin layer of rhodamine 6G (spin coated and dried on a glass coverslip), the second objective collected the fluorescence generated by the rhodamine layer, which was then recorded on a CCD camera. By changing the vertical position of the upper objective, we reconstructed the whole x-y-z distribution of the holographic excitation volume.

Daily calibration of the holographic illumination system consisted in verifying the spatial alignment between the patterns of illumination and the imaging system. In setup 2 (combining 2P CGH with widefield 1P imaging), we used the holographic patterns to excite a thin fluorescent layer and checked the position of the pattern in the field by imaging the evoked fluorescence on the camera. In setup 1 (combining 2P CGH with 2P scanning imaging), we used the holographic pattern to bleach a thick fluorescent plate (Chroma, part No. 92001) and then re-imaged the bleached pattern with the 2P scanning laser. In this way, we obtained the exact positioning of the holographic patterns in the coordinates of the imaging system. By iteratively adjusting the coordinate system of the holographic patterns (specifically, an x-y-z stretch and translation, together with a rotation in the x-y plane), we could achieve a precise overlap with the imaging coordinate system. During experiments, this calibration allowed us to use fluorescent images as a reference to place with micrometric precision photostimulation spots on the structures of interest.

Image analysis: determining the fluorescence brightness from the soma to the neurites. Images for this analysis were taken at 14–18 DIV (10–14 d after transfection) from cultured neurons. The image analysis was performed in ImageJ. For each neuron we first defined the boundaries of the soma. To that end, we drew a 20-μm-diameter circle near the soma, inside which there was no apparent fluorescence from the soma or from neurites. We defined the average fluorescence in this circle as background fluorescence. We considered pixels with fluorescence intensity of at least 10% above background levels as part of the soma and processes, and we defined the boundary between soma and processes by the cell morphology. Then we drew a polygon along the defined soma boundary, measured the average fluorescence inside it and subtracted the previously calculated background value. The resulting value was considered the soma fluorescence. To measure fluorescence intensities along the neurites, we defined 1-μm² rectangles along the neurite that were up to 100 μm away from the soma at increments of 10 μm. The distance between each rectangle and the soma was measured along the neurites (note well: this did not correspond to the minimum linear distance from the soma, since neurites are curved). We then defined the background value as described above for the soma. To be considered inside the neurite, we required that the pixel intensity values at the boundaries of the rectangle be at least 10% above background levels. We averaged the fluorescence intensity in each rectangle, subtracted the background, then divided it by the average soma fluorescence and plotted the resulting ratios with respect to their distances along the neurites. The ratios for each distance were averaged across neurites, and data were plotted (using Matlab) as average and s.e.m. (for CoChR-GFP, $n = 5$ neurites from 5 cells from 2 cultures; for soCoChR-GFP, $n = 5$ neurites from 5 cells from 3 cultures; for CoChR-Na$_V$1.2(II–III)-GFP, $n = 5$ neurites from 5 cells from 4 cultures). For the Kolmogorov–Smirnov test we verified that the dependent variable (fluorescence) was at least ordinal, that the two samples (cells expressing CoChR vs. cells expressing soCoChR) were independent and that in both cases cells were chosen randomly. Image analysis in brain slices was performed the same way; however, because of the dense labeling of cells we needed to determine the continuity of any given measured cell. Since only patched cells were labeled with Alexa 594, we verified cell continuity using the red channel and measured the fluorescence in the green (GFP) channel. This was performed for cells expressing CoChR vs. soCoChR.

Sample size determination. Because the experiments here were aimed at developing a technology, rather than testing a formal scientific hypothesis, the animal numbers in the paper were forecast on the basis of past neuroengineering projects we have done, using the experience we have attained since starting the Synthetic Neurobiology group at MIT, as done by Klapoetke et al.[19]. This follows guidelines recommended by the NIH[61] regarding "experiments based on the success or failure of a desired goal."

Data analysis. *Analyzing current amplitudes and current decay time following 1P photostimulation experiments.* For current amplitude analysis, during

photostimulation experiments, voltage clamp traces were recorded and the amplitudes of the current were taken directly from Clampfit (Molecular Devices) and copied into an Excel spreadsheet. For each patched cell, there was one current value. We averaged the photocurrent amplitude values across cells for each opsin targeting variant and calculated the s.e.m. ($n = 13$ neurons from 3 cultures and 13 neurons from 3 cultures for CoChR-GFP and soCoChR-GFP, respectively). We then performed a two-sided Wilcoxon rank sum test (in Matlab). Full statistics are in Supplementary Table 3. For the Wilcoxon rank sum test, we verified that we were comparing two independent categorical groups (the first group with cells expressing CoChR and the second group with cells expressing soCoChR), that the dependent variable (percentage) was ordinal and that observations of dependent variables were independent (because these were different experiments, on different neurons).

For τ_{off} analysis, during photostimulation experiments, voltage clamp traces were recorded and their current decay times (τ_{off}) were extracted from monoexponential fits in Clampfit (Molecular Devices). For each patched cell, there was one τ_{off} value. We averaged the τ_{off} values across cells for each opsin targeting variant and calculated the s.e.m. ($n = 13$ neurons from 3 cultures and 13 neurons from 3 cultures for CoChR-GFP and soCoChR-GFP). We then performed a two-sided Wilcoxon rank sum test (in Matlab). Full statistics are in Supplementary Table 3. For the Wilcoxon rank sum test, we verified that we were comparing two independent categorical groups (first group with cells expressing CoChR, second group with cells expressing soCoChR), that the dependent variable (percentage) was ordinal and that the observations of dependent variables were independent (because these were different experiments, on different neurons).

Analysis procedure for DMD experiments. To find the percentage of patched cells spiking when directly photostimulated, we defined the patched cell as having an AP when its membrane voltage depolarized by at least 35 mV upon photostimulation. For each of the 5 cells patched, we recorded the data as 1 if the patched cell yielded an AP when photostimulated and 0 if the patched cell did not yield an AP when photostimulated. We found the percentage of APs in patched cells resulting from direct stimulation as instances of 1 and dividing the sum by the number of patched cells ($n = 5$ cells from 4 cultures for CoChR-GFP; $n = 5$ cells from 5 cultures for CoChR-KA2(1–150)-GFP).

To find the percentage of photostimulated neighboring somata yielding an AP in the patched cell, we defined the patched cell as having an AP when its membrane voltage was depolarized by at least 35 mV upon photostimulation. The baseline was calculated as the average of the voltage values over the 100-ms period that preceded the event. For each of the 5 cells patched, 9 cells neighboring the patched cell were photostimulated. We then counted the number of neighboring cells whose stimulation led to an AP in the patched cell and divided it by the number of photostimulated neighboring cells. This value was then averaged across the 5 patched cells ($n = 5$ cells from 4 cultures for CoChR-GFP; $n = 5$ cells from 5 cultures for soCoChR-GFP). We then plotted the average percentage and s.e.m. for CoChR-GFP and soCoChR-GFP. We compared this percentage between CoChR-GFP and soCoChR-GFP via a two-sided Wilcoxon rank sum test (Matlab). Before performing the Wilcoxon rank sum test, we verified that we were comparing two independent categorical groups (first group with cells expressing CoChR, second group with cells expressing soCoChR), that the dependent variable (percentage) was ordinal and that the observations of dependent variables were independent (because these were different experiments, on different neurons).

To find the percentage of photostimulated neighboring somata yielding a depolarization in the patched cell, we defined the patched cell as having a depolarization when its membrane voltage increased from baseline by more than 0.5 mV upon photostimulation. Baseline was calculated as the average of the voltage values over the 100-ms period that preceded the event. For each of the 5 cells patched, 9 cells neighboring the patched cell were photostimulated. We then counted the number of neighboring cells whose stimulation led to a depolarization in the patched cell and divided it by the number of photostimulated neighboring cells. The value was averaged across the 5 patched cells ($n = 5$ cells from 4 cultures for CoChR-GFP; $n = 5$ cells from 5 cultures for soCoChR-GFP)). We then plotted the average percentage and s.e.m. for CoChR-GFP and soCoChR -GFP. We compared this percentage between CoChR-GFP and soCoChR-GFP by a two-sided Wilcoxon rank sum test (Matlab).

Measurement of 2P excitation spectrum. The wavelength dependence of the 2P excitation of CoChR (Supplementary Fig. 7) was measured on cultured CHO cells stimulated using the tunable laser in setup 1. To cover the entire cell body, the optical path of the imaging laser was modified to underfill the objective back aperture and generate a large 2P Gaussian excitation (FWHM = 38 μm) at the sample plane. Wavelength scanning was performed using photostimulation pulses of 200 ms at constant photon flux over the investigated wavelength range ($2.4 \pm 0.3 \times 10^{26}$ photons s^{-1} m^{-2}, defined as the time-averaged total number of photons per unit area, spatially averaged over the Gaussian spot surface). Laser pulse width is assumed to be constant across wavelengths. From the photocurrent curves, we extracted the wavelength dependence of the peak currents and of the exponential rise and decay times, which we used to deduce the normalized excitation cross-section spectrum (Supplementary Fig. 7b) using equation (13) from Chaigneau et al.[10].

Modeling of the power dependence of the axial resolution of 2P holographic photostimulation. The nonlinear opsin response to the illumination power can affect the effective axial resolution of photostimulation. To evaluate and model this effect, we first recorded the response of a CoChR-expressing CHO cell to different 2P holographic illumination powers (shown in the inset of Supplementary Fig. 8d). The use of cultured CHO cells, in contrast to neurons, allowed us to avoid any influence of excitation of neurites around the soma. As expected, the photoinduced peak currents at high excitation power showed saturation as power increased. In a first approximation, the curve of the normalized peak current near saturation could be fitted with an exponential curve: $I(P) = 1 - e^{-P/P'}$, with $P' \approx 0.06$ mW/μm^2 ($\lambda = 1{,}030$ nm, setup 1). Second, we extracted the normalized intensity axial profile $p(z)$ of the excitation holographic spot from a Gaussian fit of the corresponding axial fluorescence profile (Supplementary Fig. 8b,c). Finally we modeled the axial profile of the photocurrent by using the expression $I(z) = 1 - e^{-P_0 p(z)/P'}$, with P_0 the nominal power density (per unit surface) at $z = 0$. The results of the model are reported and compared with experimental results in Supplementary Fig. 8d,e.

A further optimization of the model would include a more precise fit of the quadratic behavior of the photocurrent at low power, far below saturation, and would also consider the convolution of the illumination profile with the exact morphology of the neuron cell body (here considered simply as a thin disk) and the spatial distribution of its axon and dendritic tree.

Analyzing photocurrent integrals under photostimulation along neurites. For each photostimulation location, 1 to 3 trials were acquired and the resulting traces were averaged. The current integral over time was calculated by integrating the current response recorded at the soma in voltage-clamp configuration from the onset of the photostimulation until the time of recovery to the initial resting value of the current. In the calculation of the integral, an offset in the current curve was introduced corresponding to the integral of the holding current at rest.

The distance from the soma was estimated on the basis of the coordinates of the photostimulation spots placed along neurites. This sequence was manually defined during the experiment and consisted of a series of 10-μm spots starting from the center of the soma and moving away from it along a neurite with a step of approximately 10 μm up to a maximum distance of 100 μm from the soma (while taking into account the curvature of neurites). Post-experimentally, the distance between each pair of consecutive spots d_i was defined as the Cartesian distance between the center of the consecutive spots (taking into account the x, y and z coordinate of each). The distance to the soma from the ith spot was then calculated as

$$\sum_{j=1}^{i-1} d_j$$

The photostimulation sequence was then performed starting from the most peripheral spot on the neurites to the spot on the soma.

Current integrals over time at various neurite locations were normalized to the current integral recorded at the soma. The current integral values were then binned according to their distance from soma in intervals of 15 μm. Values were averaged across neurites (1 to 3 neurites per cell were investigated) and data plotted as mean ± s.e.m. (Fig. 3). To estimate the statistical significance of the difference between CoChR-GFP and soCoChR-GFP photocurrents, we performed a two-sample Bonferroni-corrected Kolmogorov–Smirnov test for each binning interval. The test was two-sided. For the Kolmogorov–Smirnov test we verified that the dependent variable (photocurrent integral) was at least ordinal, that the two samples (cells expressing CoChR vs. cells expressing soCoChR) were independent and that both samples were random (neurons and neurites to study were chosen randomly).

Results of the test are reported in Supplementary Table 4. Data were analyzed using pClamp10 software (Molecular Devices), IgorPro and Matlab (MathWorks, Inc.).

Analyzing single- and multiple-soma holographic stimulations in brain slices. For each patched cell, we counted the number of neighboring cells whose stimulation led to an AP in the patched cell, divided this number by the number of photostimulated neighboring cells and then averaged this ratio across all patched cells. Data are presented as mean ± s.e.m. in Fig. 5. Significance was tested with the non-parametric two-sided Wilcoxon rank sum test (Matlab) for continuous variable (percentage) in Fig. 5e and the non-parametric χ^2 test for discrete values in Fig. 5g. For the Wilcoxon rank sum test, we verified that we were comparing two independent categorical groups (cells expressing CoChR and soCoChR), that the dependent variable (percentage) was ordinal and that observations of dependent variables were independent (since obtained on different experiments and different neurons). For the χ^2 test, we verified that variables were mutually exclusive and that the studied groups were independent (cells expressing CoChR and soCoChR).

For simultaneous stimulation experiments, we calculated the percentage of patched cells firing a single AP or multiple APs when their neighbors were simultaneously stimulated. Illumination patterns were composed of 5 to 8 holographic spots. The results were averaged across the patched cells.

Connectivity experiments were performed by sequentially photostimulating presynaptic cells. The whole photostimulation sequence was repeated three times. The postsynaptic traces from the three trials were averaged for analysis and for the traces reported in the figures. Whenever stimulation of presynaptic cell elicited a current (I_{TOT}) in the patched cell, we defined the artifactual component, I_{ART}, as the residual current left after application of synaptic blockers. The PSC component was then calculated as PSC = I_{TOT} − I_{ART}. The ratio PSC/I_{ART} was used to compare connectivity experiments performed using soCoChR-GFP and CoChR-GFP. Data are presented as mean ± s.e.m. in Fig. 6. Data were analyzed using pClamp10 software (Molecular Devices), IgorPro and R-studio.

Excluding data points. For recording in slices, data points (singular trials) were excluded if the recording was unstable, meaning the baseline potential changed by more than 5 mV during the recording. Cells were excluded if a gigaohm seal was lost or a high leak current appeared.

For recording in culture, data points (cells) were excluded if we could not establish a gigaohm seal.

Statistics. For comparison of GFP brightness vs. position along the neurite between constructs, two-sample Kolmogorov–Smirnov (K-S) tests with Bonferroni correction were performed. For comparing spike probability vs. irradiance, Bonferroni-corrected Wilcoxon rank sum tests were used. For comparisons of normalized integrated photocurrent along neurites, two-sample K-S tests with Bonferroni correction were used. For comparing of the average distances between patched cells and photostimulated cells, Wilcoxon rank sum tests were performed. For comparing single and multiple spike probabilities, the χ^2 test was used. Wilcoxon rank sum tests were used for comparison of PSC and I_{ART} currents and for comparison of the PSC/I_{ART} ratios. Data collection and analysis were not performed blind to the conditions of the experiments. Animals and cultures were randomly assigned to the different experimental groups. Information about the experimental design and statistics are given in the Life Sciences Reporting Summary. Normality and equal variances were not assumed, and therefore all tests were non-parametric (K-S test, χ^2 test, Wilcoxon rank sum test).

Accession codes. GenBank: SoCoChR-GFP, MF795583; KA2(1–150), MF795584.

Life Sciences Reporting Summary. Further information on experimental design is available in the Life Sciences Reporting Summary.

Data availability. All relevant data are available from the authors upon reasonable request. Sequences are available in the Supplementary Note. Clones will be made available through the nonprofit DNA distributor Addgene, as well as the University of North Carolina and University of Pennsylvania viral cores.

References

47. Jiang, M. & Chen, G. High Ca²⁺-phosphate transfection efficiency in low-density neuronal cultures. *Nat. Protoc.* **1**, 695–700 (2006).
48. Chow, B. Y. et al. High-performance genetically targetable optical neural silencing by light-driven proton pumps. *Nature* **463**, 98–102 (2010).
49. Ma, D. et al. Role of ER export signals in controlling surface potassium channel numbers. *Science* **291**, 316–319 (2001).
50. Hofherr, A., Fakler, B. & Klöcker, N. Selective Golgi export of Kir2.1 controls the stoichiometry of functional Kir2.x channel heteromers. *J. Cell Sci.* **118**, 1935–1943 (2005).
51. Ducros, M. et al. Efficient large core fiber-based detection for multi-channel two-photon fluorescence microscopy and spectral unmixing. *J. Neurosci. Methods* **198**, 172–180 (2011).
52. Lutz, C. et al. Holographic photolysis of caged neurotransmitters. *Nat. Methods* **5**, 821–827 (2008).
53. Gerchberg, R. & Saxton, W. A practical algorithm for the determination of the phase from image and diffraction plane pictures. *Optik* **35**, 237 (1972).
54. Haist, T., Schönleber, M. & Tiziani, H. J. Computer-generated holograms from 3D-objects written on twisted-nematic liquid crystal displays. *Opt. Commun.* **140**, 299–308 (1997).
55. Hernandez, O., Guillon, M., Papagiakoumou, E. & Emiliani, V. Zero-order suppression for two-photon holographic excitation. *Opt. Lett.* **39**, 5953–5956 (2014).
56. Golan, L., Reutsky, I., Farah, N. & Shoham, S. Design and characteristics of holographic neural photo-stimulation systems. *J. Neural Eng.* **6**, 066004 (2009).
57. Yang, S. et al. Three-dimensional holographic photostimulation of the dendritic arbor. *J. Neural Eng.* **8**, 046002 (2011).
58. Conti, R., Assayag, O., de Sars, V., Guillon, M. & Emiliani, V. Computer generated holography with intensity-graded patterns. *Front. Cell. Neurosci.* **10**, 236 (2016).
59. Mütze, J. et al. Excitation spectra and brightness optimization of two-photon excited probes. *Biophys. J.* **102**, 934–944 (2012).
60. Horton, N. G. et al. In vivo three-photon microscopy of subcortical structures within an intact mouse brain. *Nat. Photonics* **7**, 205–209 (2013).
61. Dell, R. B., Holleran, S. & Ramakrishnan, R. Sample size determination. *ILAR J.* **43**, 207–213 (2002).

naturereasearch

Corresponding author(s):   Ed Boyden and Valentina Emiliani

☐ Initial submission   ☐ Revised version   ☒ Final submission

Life Sciences Reporting Summary

Nature Research wishes to improve the reproducibility of the work that we publish. This form is intended for publication with all accepted life science papers and provides structure for consistency and transparency in reporting. Every life science submission will use this form; some list items might not apply to an individual manuscript, but all fields must be completed for clarity.

For further information on the points included in this form, see Reporting Life Sciences Research. For further information on Nature Research policies, including our data availability policy, see Authors & Referees and the Editorial Policy Checklist.

▶ Experimental design

1. Sample size

Describe how sample size was determined.

> The explanation for sample size is given in the manuscript, under "Sample size determination" (p. 43).
>
> Because the experiments here were aimed at developing a technology, rather than testing a formal scientific hypothesis, the animal numbers in the paper were forecasted based upon past neuroengineering projects we have done, using the experience we have attained since starting the Synthetic Neurobiology group at MIT, similar to Klapoetke et al19. This follows guidelines recommended by the NIH63 regarding "experiments based on the success or failure of a desired goal."

2. Data exclusions

Describe any data exclusions.

> For recording in slices, data points (singular trials) were excluded if the recording was unstable, meaning the baseline potential changed by more than 5 mV during the recording. Cells were excluded if a gigaohm seal was lost or a high leak current appeared.

3. Replication

Describe whether the experimental findings were reliably reproduced.

> For every experiment we conducted, we repeated it several time and then conducted a statistical test to check for an experimental effect. Reliability led to statistical significance.

4. Randomization

Describe how samples/organisms/participants were allocated into experimental groups.

> Animals and cultures were randomly assigned to the different experimental groups.
>
> It appears in the methods section, paragraph " Randomization".

5. Blinding

Describe whether the investigators were blinded to group allocation during data collection and/or analysis.

> There were no blind experiments.

Note: all studies involving animals and/or human research participants must disclose whether blinding and randomization were used.

6. Statistical parameters

For all figures and tables that use statistical methods, confirm that the following items are present in relevant figure legends (or in the Methods section if additional space is needed).

n/a	Confirmed	
☐	☒	The <u>exact sample size</u> (*n*) for each experimental group/condition, given as a discrete number and unit of measurement (animals, litters, cultures, etc.)
☐	☒	A description of how samples were collected, noting whether measurements were taken from distinct samples or whether the same sample was measured repeatedly
☐	☒	A statement indicating how many times each experiment was replicated
☐	☒	The statistical test(s) used and whether they are one- or two-sided (note: only common tests should be described solely by name; more complex techniques should be described in the Methods section)
☐	☒	A description of any assumptions or corrections, such as an adjustment for multiple comparisons
☐	☒	The test results (e.g. *P* values) given as exact values whenever possible and with confidence intervals noted
☐	☒	A clear description of statistics including <u>central tendency</u> (e.g. median, mean) and <u>variation</u> (e.g. standard deviation, interquartile range)
☐	☒	Clearly defined error bars

See the web collection on statistics for biologists for further resources and guidance.

▶ Software

Policy information about availability of computer code

7. Software

Describe the software used to analyze the data in this study.	Software used: Matlab, origin8, IgorPro, pClamp10, Excel.

For manuscripts utilizing custom algorithms or software that are central to the paper but not yet described in the published literature, software must be made available to editors and reviewers upon request. We strongly encourage code deposition in a community repository (e.g. GitHub). *Nature Methods* guidance for providing algorithms and software for publication provides further information on this topic.

▶ Materials and reagents

Policy information about availability of materials

8. Materials availability

Indicate whether there are restrictions on availability of unique materials or if these materials are only available for distribution by a for-profit company.	We provided a Data availability statement (p.14-15): "All relevant data are available from the authors. Sequences are available in this manuscript under Supplementary information. Clones will be made available through the nonprofit DNA distributor Addgene, as well as the UNC and UPenn Viral cores".

9. Antibodies

Describe the antibodies used and how they were validated for use in the system under study (i.e. assay and species).	No antibodies were used in our study.

10. Eukaryotic cell lines

a. State the source of each eukaryotic cell line used.	Chinese hamster ovary (CHO) ordered from Sigma-Aldrich, subclones of the parental CHO cell line originated by Puck in 1957 (The Journal of experimental medicine, 108, (1958-12-1)).
b. Describe the method of cell line authentication used.	Not known; presumably standard Sigma-Aldrich procedures were followed. Cells lot number 10D001
c. Report whether the cell lines were tested for mycoplasma contamination.	Cell lines were tested with Hoechst method.
d. If any of the cell lines used are listed in the database of commonly misidentified cell lines maintained by ICLAC, provide a scientific rationale for their use.	CHO cells are not in the list.

▶ Animals and human research participants

Policy information about studies involving animals; when reporting animal research, follow the ARRIVE guidelines

11. Description of research animals

Provide details on animals and/or animal-derived materials used in the study.

Species: the species of animals were reported in in the Methods, under "Viral injections and whole-cell electrophysiology in brain slices" (p.33) and "Primary neuron culture, transfection and transduction " (p.29).

Strain: the strain of animals strains were well-characterized mice strains appearing in multiple publications from multiple labs.

Sex: for slice experiments we used male mice, and mentioned it under "Viral injections and whole-cell electrophysiology in brain slices".
For cultures, we do not know the sex of the mice used for the experiments.

Age: reported in the Methods, under "Viral injections and whole-cell electrophysiology in brain slices" and "Primary neuron culture, transfection and transduction ".

Policy information about studies involving human research participants

12. Description of human research participants

Describe the covariate-relevant population characteristics of the human research participants.

N/A

In the format provided by the authors and unedited.

Temporally precise single-cell-resolution optogenetics

Or A. Shemesh[1,2,3,4,5]**, Dimitrii Tanese**[6]**, Valeria Zampini**[6,7]**, Changyang Linghu**[1,2,3,4,5]**, Kiryl Piatkevich**[1,2,3,4,5]**, Emiliano Ronzitti**[6,7]**, Eirini Papagiakoumou** [6,8]**, Edward S. Boyden** [1,2,3,4,5]***** **and Valentina Emiliani** [6]*****

[1]Media Laboratory, Massachusetts Institute of Technology (MIT), Cambridge, MA, USA. [2]Department of Biological Engineering, MIT, Cambridge, MA, USA. [3]Center for Neurobiological Engineering, MIT, Cambridge, MA, USA. [4]Department of Brain and Cognitive Sciences, MIT, Cambridge, MA, USA. [5]McGovern Institute for Brain Research, MIT, Cambridge, MA, USA. [6]Neurophotonics Laboratory, Wave Front Engineering Microscopy Group, CNRS UMR8250, Université Paris Descartes, Paris, France. [7]Institut de la Vision, UM 80, UPMC, Paris, France. [8]Institut national de la santé et de la recherche médicale (Inserm), Paris, France. Or A. Shemesh, Dimitrii Tanese and Valeria Zampini contributed equally to this work. *e-mail: esb@media.mit.edu; valentina.emiliani@parisdescartes.fr

Supplementary Figure 1

An N-terminal domain of kainate receptor subunit 2 is retained in the soma.

(**a**) A hippocampal neuron expressing GFP. (**b**) A hippocampal neuron expressing KA2-GFP. (**c**) A hippocampal neuron expressing KA2(1-150)-GFP. Scale bars for **a-c**: 50 µm. (**d, e, f**) Box-and-whiskers plots of GFP brightness versus position along a neurite, normalized to GFP brightness at the soma for GFP (n=5 neurites from 3 cells), KA2-GFP (n=5 neurites from 3 cells) and KA2(1-150)-GFP (n=5 neurites from 3 cells) respectively. Red line denotes the median. Top and bottom edges of the box indicate the 75th and 25th percentiles, respectively. Top and bottom whiskers indicate the highest and lowest values respectively. See **Supplementary Table 2** for Bonferroni-corrected Kolmogorov-Smirnov tests for **Figure S1**.
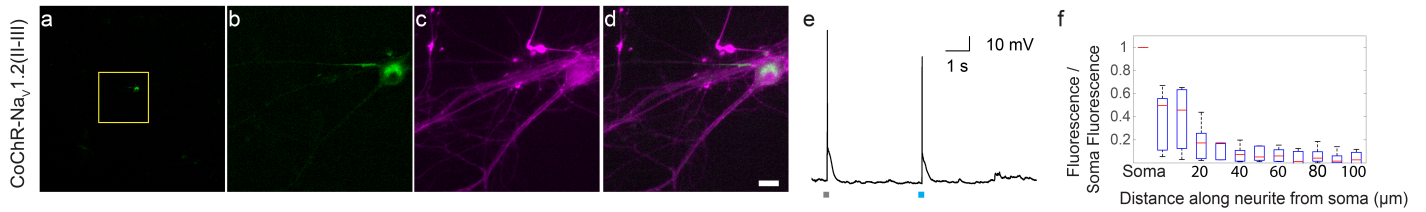
Supplementary Figure 2

CoChR-Na$_V$1.2(II–III)-GFP expression and photostimulation in cultured hippocampal neurons.

(**a-d**) Images are presented for cultured hippocampal neurons expressing CoChR-Na$_V$1.2(II-III)-GFP, along with the countermarker mCherry. (**a**) A hippocampal neuron in culture expressing CoChR-Na$_V$1.2(II-III)-GFP and mCherry, seen in the GFP channel (scale bar: 100 μm). (**b**) Zoomed-in image from the yellow rectangle of **a**. (**c**) The neuron of **b,** seen in the mCherry channel (magenta), along with other nearby neurons. (**d**) Merge of **b** and **c** (scale bar for **b-d**: 20 μm). (**e**) Whole cell current clamp recording of a cultured hippocampal neuron expressing CoChR-Na$_V$1.2(II-III)-GFP, under current injection (10 ms duration; gray rectangle) and optical stimulation (480nm, 34.84mW/mm^2, 1 ms duration; blue rectangle). Rectangles not to scale. (**f**) Box-and-whiskers plot of GFP brightness versus position along a neurite, normalized to GFP brightness at the soma, extracted from neurites of cultured hippocampal neurons expressing CoChR-Na$_V$1.2(II-III)-GFP (n = 5 neurites taken from 5 cells from 4 cultures). Red line denotes the median. Top and bottom edges of the box indicate the 75th and 25th percentiles, respectively. Top and bottom whiskers indicate the highest and lowest values respectively.

Ai CoChR-GFP-Kv2.1$_{motif}$

Aii CoChR-GFP-Kv2.1$_{motif}$

B CoChR-GFP-Kv2.1$_{motif}$
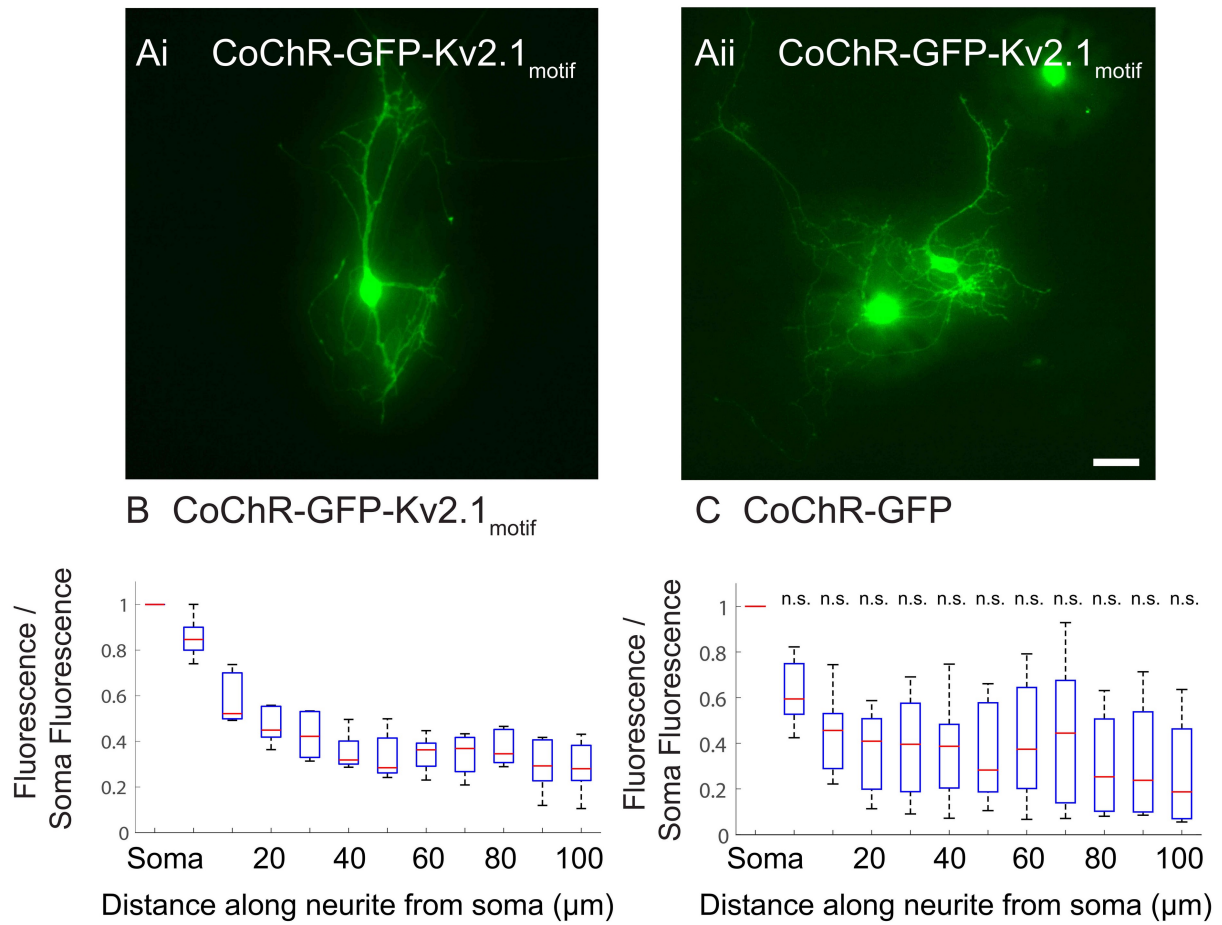
C CoChR-GFP

Supplementary Figure 3

CoChR-GFP-Kv2.1-motif expression is somatodendritic.

(Ai, Aii) Hippocampal neurons expressing CoChR-GFP-Kv2.1$_{motif}$. **(B, C)** Box-and-whisker plots of brightness versus position along a neurite, normalized to brightness at the soma for CoChR-GFP-Kv2.1$_{motif}$ (**B**, n = 5 neurites from 5 cells from 2 cultures) and CoChR-GFP (**C**, n = 7 neurites from 5 cells from 2 cultures). Top and bottom edges of the box indicate the 75th and 25th percentiles, respectively. Red line denotes the median. Top and bottom whiskers indicate the highest and lowest values respectively. n.s., not significant, comparing **B** vs. **C**; see **Supplementary Table 3** for Bonferroni-corrected Kolmogorov-Smirnov tests for **Figure S3**. Scale bar: 20μm.
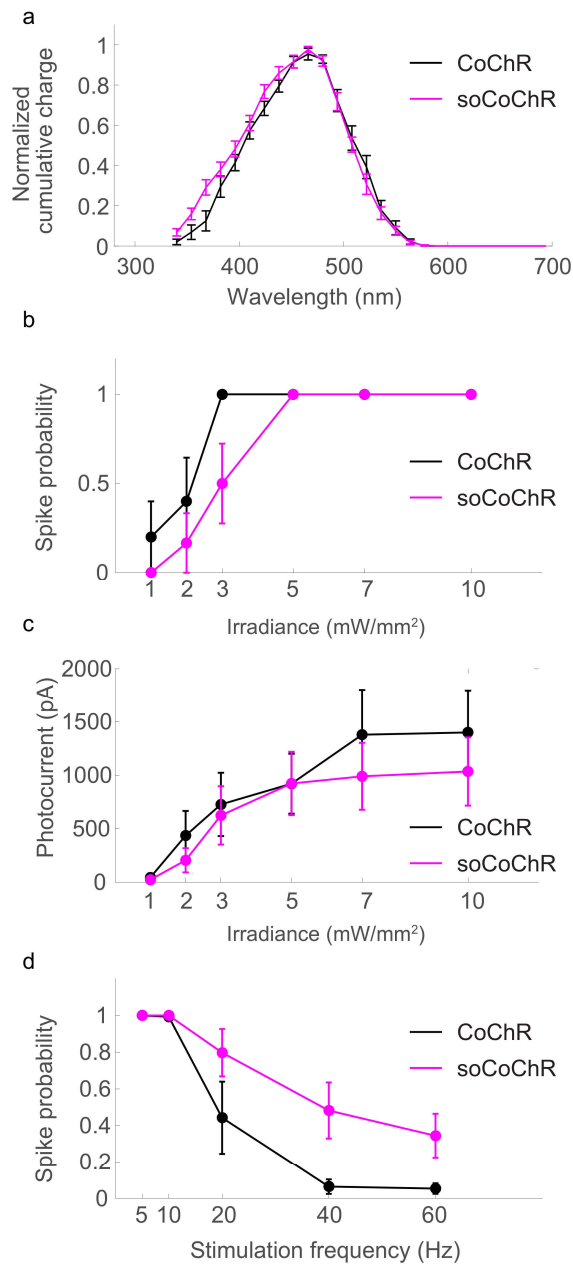
Supplementary Figure 4

In vitro single photon characterization of CoChR and soCoChR.

(**a**) Action spectra for CoChR (n = 9 cells) and soCoChR (n = 10 cells) measured in cultured neurons. Plotted data are mean ± s.e.m. (**b**) Blue light driven spike probability as a function of irradiance for CoChR (magenta) and soCoChR (black) expressing cells. Plotted data are mean ± s.e.m (n = 6 cells for each opsin). All blue light spiking protocols used 2 ms width light pulses at 480 nm. (**c**) Blue light driven photocurrents as a function of irradiance for CoChR (magenta) and soCoChR (black) expressing cells. Plotted data are mean ± s.e.m (n = 7 cells for each opsin). All blue light protocols used 2 ms pulse width at 480 nm. **(d)** Blue light driven spike fidelity for CoChR (magenta) and soCoChR (black) expressing cells. All blue light spiking protocols used a train of 40 pulses, 2 ms pulse width, at 480 nm, at 5 mW/mm^2. Plotted data are mean ± s.e.m (n = 7 – 10 cells for each opsin). See **Supplementary Table 3** for full statistics for **Figure S4**.
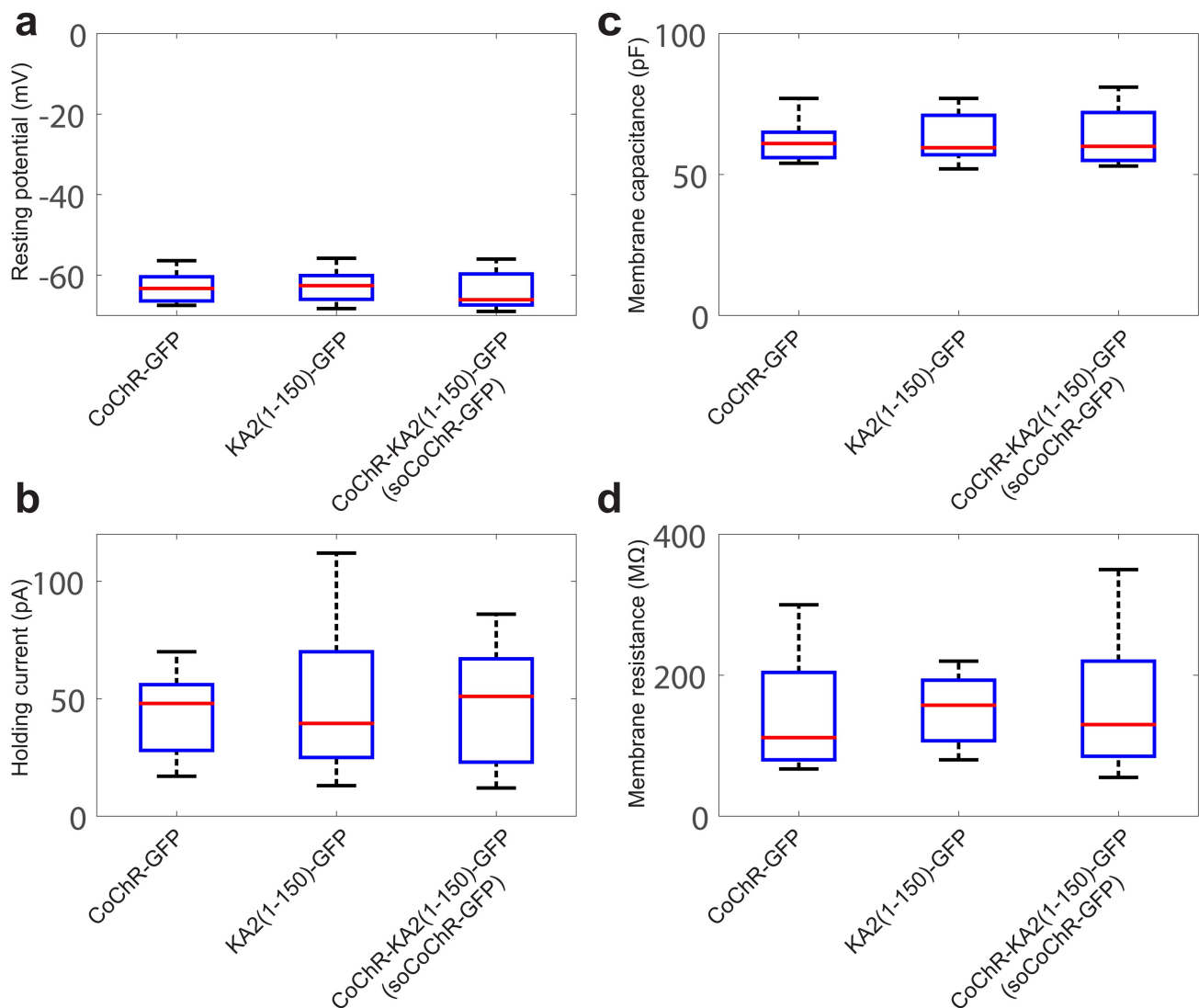
Supplementary Figure 5

Membrane properties of neurons expressing somatic vs. untargeted molecules.

Cultured hippocampal neurons expressing CoChR-GFP (n = 10 cells from 3 cultures), KA2(1-150)-GFP (n = 10 cells from 3 cultures), and soCoChR-GFP (n = 10 cells from 3 cultures) were patched 14 days following AAV transduction. (**a**) Resting potential. We performed a Kruskal-Wallis Test (not significant, P = 0.7549, chi-square = 0.5624). (**b**) Holding current. Kruskal-Wallis Test, not significant, P = 0.9875, chi-square = 0.0252. (**c**) Membrane capacitance. Kruskal-Wallis Test, not significant, P = 0.9817, chi-square = 0.0369. (**d**) Membrane resistance. Kruskal-Wallis Test, not significant, P = 0.9205, chi-square = 0.1656. For all panels, red line denotes the median. Top and bottom edges of the box indicate the 75th and 25th percentiles, respectively. Top and bottom whiskers indicate the highest and lowest values.

Setup 1

IR-CCD

1030 nm/250 fs/500 kHz
pulsed beam

L1 L2 M1 M3 *(movable)* D1 L8 M4

L/2 PC GM L7 L6 PC

2 CL L3 L4 L5 M2 L/2

SLM Ti:Sa

L9

D4 D2

CCD LED L10

D4 F1

PMT F2 F3 Fiber D3 *(movable)*

PMT OBJ

C

M5 LED

Setup 2

sCMOS

920 nm/100 fs/80 MHz
pulsed beam

Ti:Sa PoC L1 L2 M1 L5

F3

D2 Monochromator

F2

Arc lamp

CL L3 L4 D1

SLM

Olympus BX51WI

OBJ

F1

Lamp
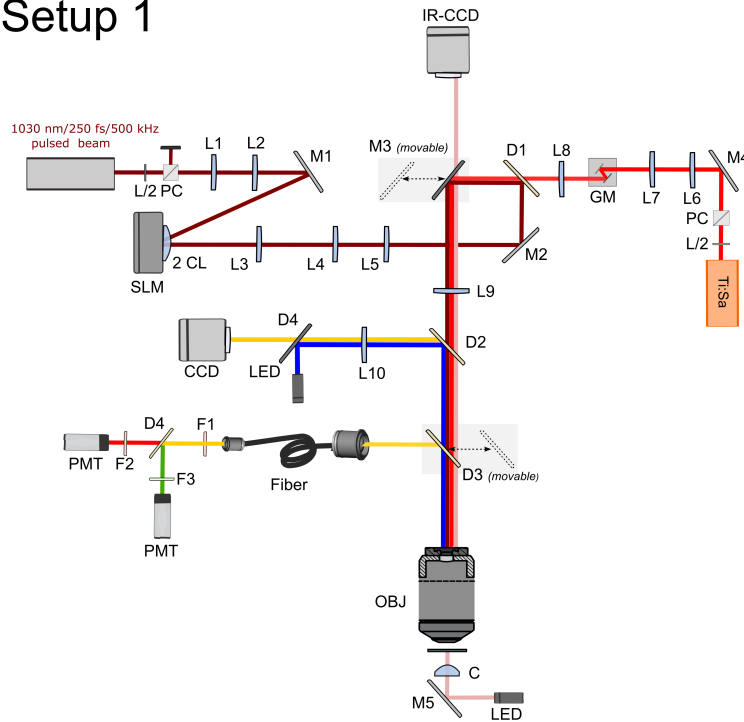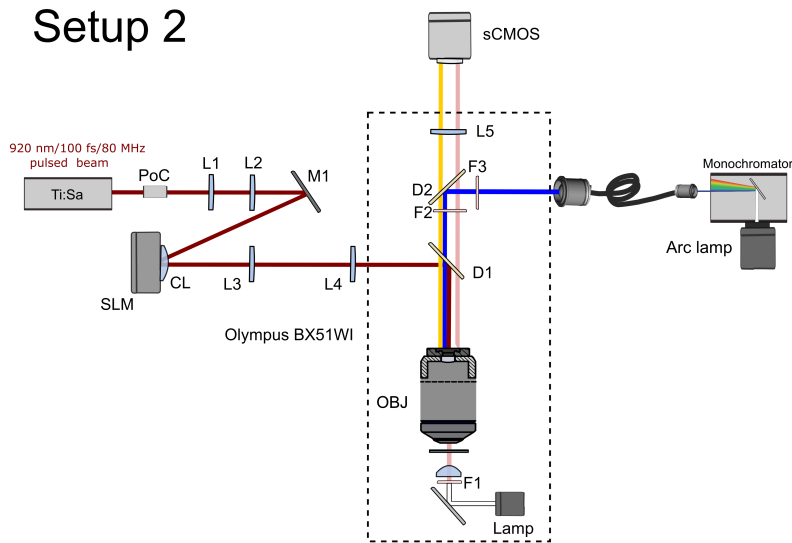
Supplementary Figure 6

Detailed schematics of the holographic microscopes, for both setup 1 and setup 2.

PC, Polarizer Cube; L/2, Half Wave Plate; M, Mirror; L, Lens; SLM, Spatial Light Modulator; CL, Cylindrical Lens; D, Dichroic; GM, Galvanometric Mirrors; F, Filter; OBJ, Objective; C, Condenser; PoC, Pockels Cell; CCD, charge-coupled device; sCMOS, scientific complementary metal-oxide semiconductor camera. See detailed description in Methods section.
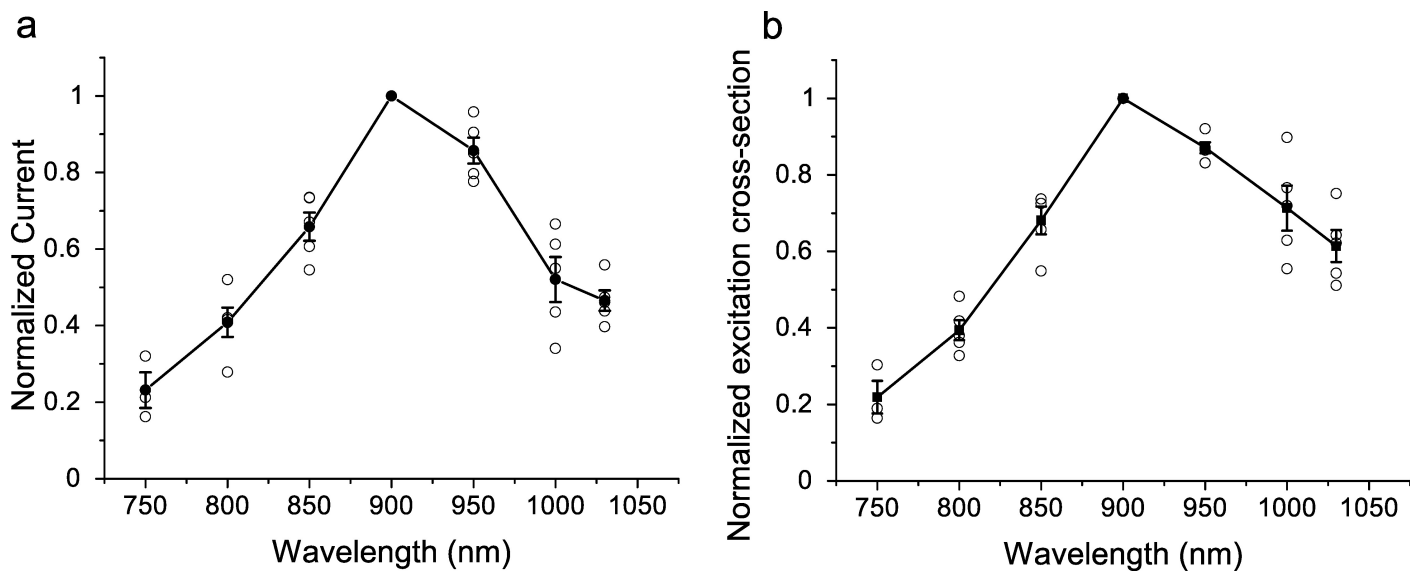
Supplementary Figure 7

2P action spectrum and normalized excitation cross section of CoChR.

(**a**) Normalized peak current of CoChR as a function of wavelength, measured in cultured CHO cells. Photostimulation was performed using a 2P Gaussian spot (FWHM=38 μm) at different wavelengths, at constant photon flux ($2.4 \pm 0.3 \ 10^{26}$ photons/s·m²) over the investigated wavelength range. Plotted data are mean ± s.e.m., with raw data in open circles, n=5 cells. (**b**) Normalized 2P excitation cross section, extracted from the photocurrent kinetics (see Methods). Plotted data are mean ± s.e.m., with raw data in open circles, n=5 cells.
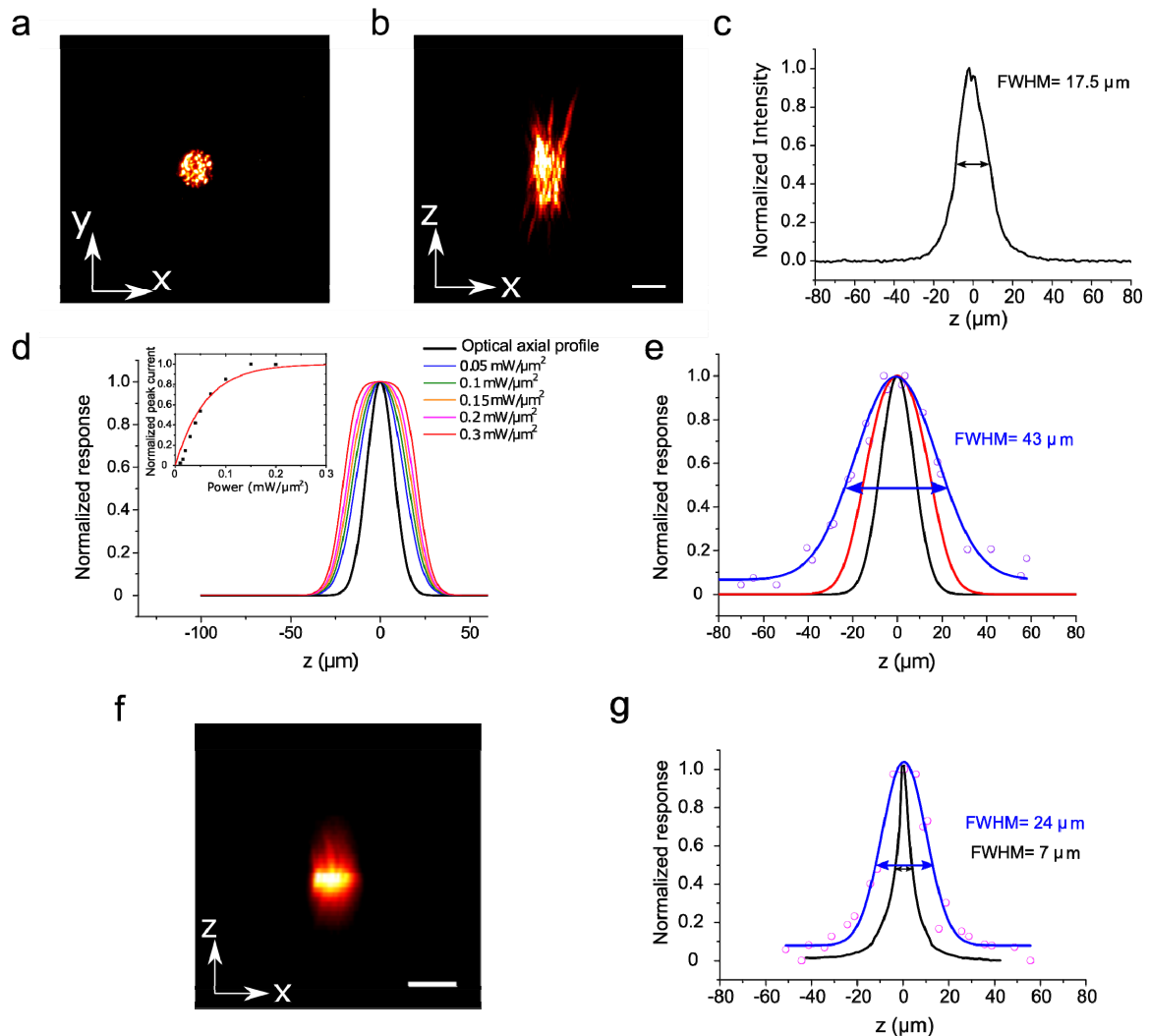
Supplementary Figure 8

Axial resolution of 2P holographic spots.

Top (**a**) and lateral (**b**) view of the fluorescence emission generated by a 10 µm diameter holographic spot on a thin fluorescent layer. The fluorescence is collected by a second bottom objective and relayed to a CCD camera; the z-stack is acquired by scanning the vertical position of the upper objective. Scale bar, 10 µm. Measured performed on setup 1 (λ=1030 nm). (**c**) Normalized axial intensity profile from the z-stack of panel **b**. (**d**) Simulated axial dependence of the photocurrent's peak at different excitation powers using the excitation spot of panels **a,b**. The black curve represents a Gaussian fit of the spot's axial profile shown in panel **c** (FWHM=17.5 µm). Colored curves represent the simulated axial dependence of the photocurrent for different excitation powers, taking into account the experimental photocurrent dependence on the excitation power shown in the inset (see Methods for more details on the model used) Inset: Black dots represent measured normalized photocurrent from a CoChR expressing CHO cell (λ=1030 nm, setup 1), fitted by an exponential (red curve). (**e**) Experimental (violet dots; n=2 CoChR expressing cells) and simulated (red line) photocurrent's peak axial profile for the 10 µm diameter holographic spot of panels **a,b** using an excitation power of 80 µW/µm^2. The blue curve is a Gaussian fit of the experimental data (FWHM=43 µm). The black curve represents the Gaussian fit of the spot's axial profile shown in panel **c**. (**f**) Lateral (x,z) view of the fluorescence emission generated by a 10 µm diameter holographic temporally focused spot on a thin fluorescent layer. Scale bar, 10 µm. Measurement performed on setup 2, modified by adding a diffraction grating for temporal focusing. (**g**) Experimental (violet dots) axial dependence of the photocurrent's peak and Gaussian fit (blue line) generated by using the temporally focused spot shown in (**f**) (n=1 CoChR expressing cell; n=1 soCoChR expressing cell). The black curve represents the optical axial resolution of the temporally focused spot of panel **f**.

(a) CoChR-GFP
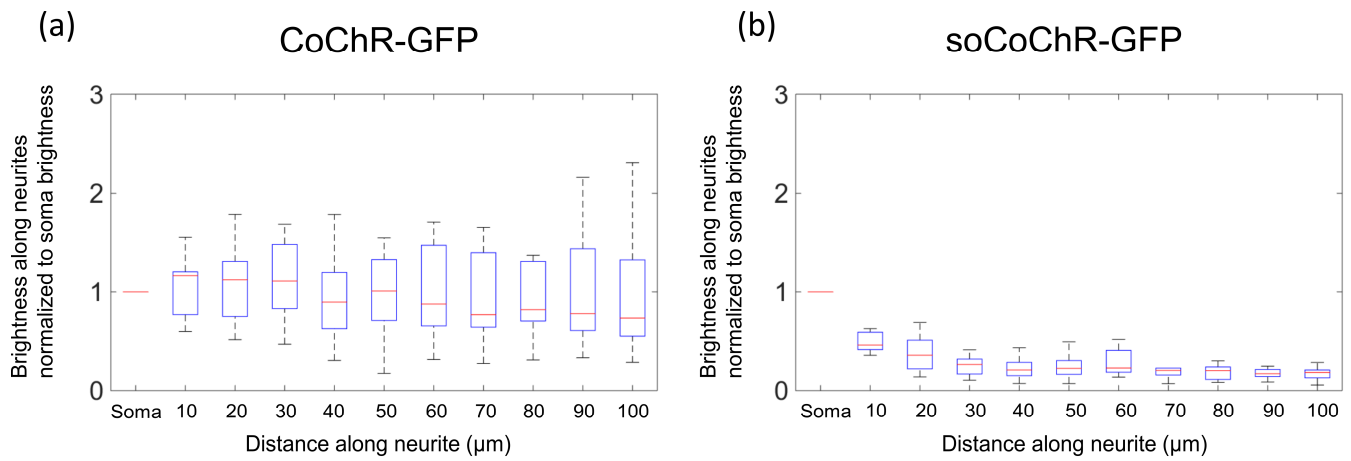
(b) soCoChR-GFP

Supplementary Figure 9

Fluorescence plots along neurites, for cells expressing CoChR-GFP or soCoChR-GFP in slices.

(a-b) Box-and-whiskers plots of GFP intensity versus position along a neurite, normalized to GFP intensity at the soma, extracted from 2P images (setup 1) of neurites of (**a**) CoChR-GFP (n = 9 neurites taken from 4 cells from 3 slices from 3 mice) and (**b**) CoChR-KA2(1-150)-GFP expressing cells (soCoChR-GFP; n = 9 neurites taken from 6 cells from 2 slices from 2 mice) in acute slices. Red line denotes the median. Top and bottom edges of the box indicate the 75th and 25th percentiles, respectively. Top and bottom whiskers indicate the highest and lowest values, respectively. For CoChR the GFP fluorescence decays slower than the corresponding current (**Fig. 3e**); this is probably due to a contribution to the fluorescence from the dense distribution of out of focus processes from neighbouring cells.
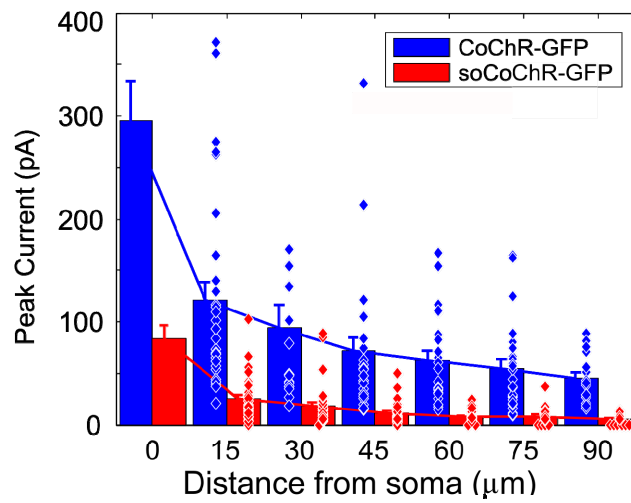
Supplementary Figure 10

Absolute currents at different distances from the soma for CoChR- and soCoChR-expressing cells in slices.

A bar plot showing the peak currents induced by illumination of neurites at different distances from the soma (corresponding to experiments reported in **Fig. 3e**), for CoChR-GFP (blue bars) and soCoChR-GFP (red bars) -expressing neurons. Bars represent mean ± s.e.m.; dots denote values for single neurites.
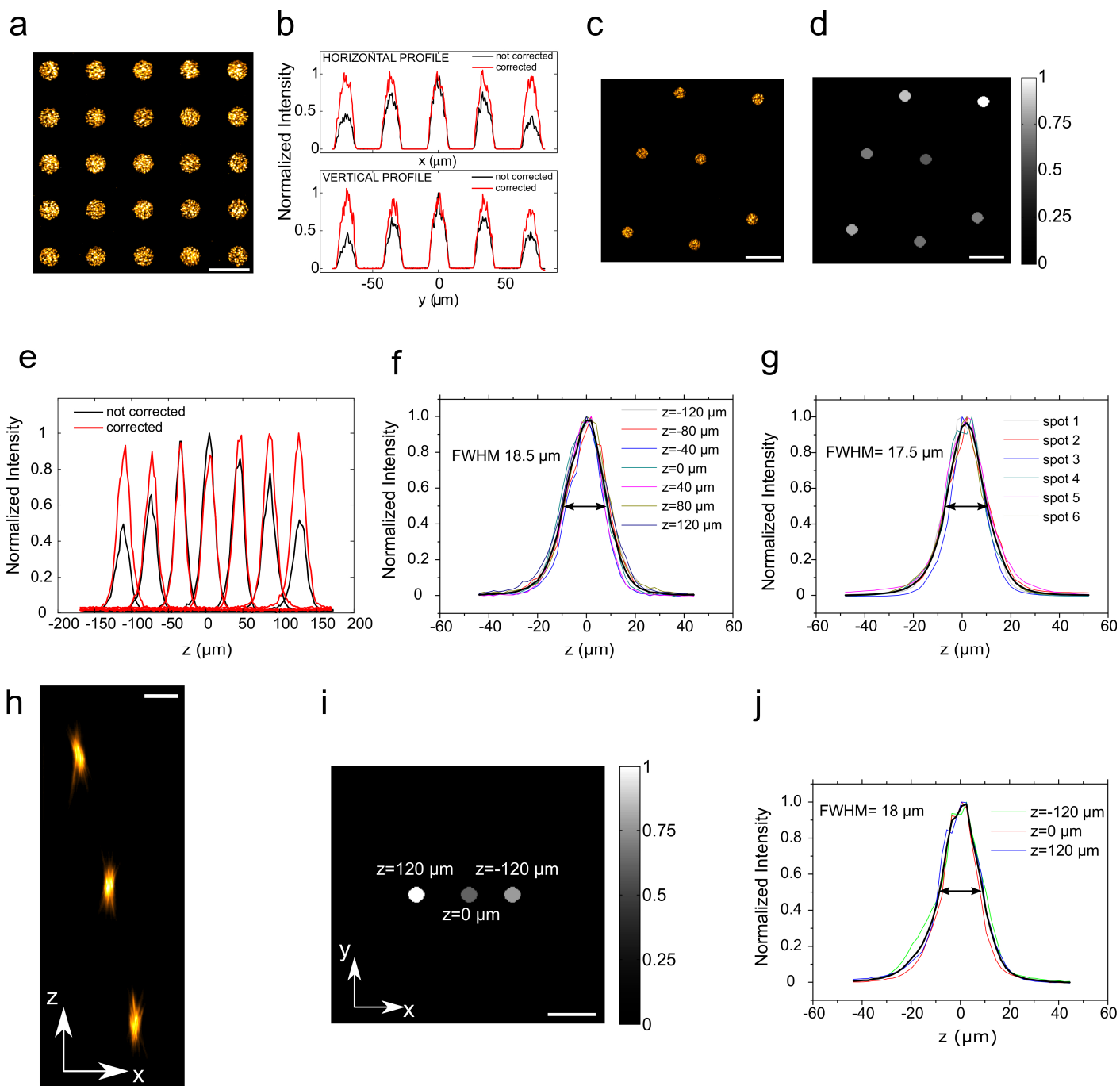
Supplementary Figure 11

Multi-spot holographic illumination and diffraction efficiency correction.

(**a**) Max projection of the fluorescence generated by a sequence of 15 μm diameter holographic spots placed on a square grid. The generation of a variable size (from 0 to 15 μm) correction holographic spot (not shown) is applied to correct for the position-dependent diffraction efficiency (see Methods). Scale bar: 30 μm. (**b**) Vertical and horizontal intensity profiles corresponding to panel **a** with and without the correction of diffraction efficiency, averaged over the 5 columns and lines of the matrix, respectively. (**c**) Fluorescence generated by the simultaneous projection of 7 randomly placed holographic spots with equal intensity, corrected for diffraction efficiency. Scale bar: 30 μm. (**d**) Graded input pattern used to calculate the hologram generating the illumination pattern in panel **c** (see

Methods). Scale bar: 30 µm. (**e**) Axial intensity profile of the fluorescence induced by a 10 µm holographic spot displaced over different axial positions relative to the microscope objective focal plane without diffraction efficiency correction (black curves) and with the correction (red curve) using an external correction spot (not shown). (**f**) Superposition of the axial intensity profiles of panel **e** (with correction of diffraction efficiency), after being centered at z=0. The black curve represents the average profile with FWHM= 18.5 µm. (**g**) Axial intensity profile of the multispot holographic pattern reported in **Figure 5b**. The black curve represents the average profile with FWHM=17.5 µm. (**h**) Lateral view of the 3D fluorescence pattern generated by 3 holographic spots (diameter 10 µm) of equal intensity at axial positions of z = -120 µm; 0; +120µm. Scale bar: 30 µm. (**i**) Graded input pattern used to calculate the hologram generating the illumination pattern in panel **h**. As in panel **d**, different input intensities were assigned to each spot to compensate for the diffraction efficiency dependence on the vertical position and to obtain the same output power density on each spot. (**j**) Superposition of the axial intensity profiles of the spots of panel **h**. The black curve represents the average profile with FWHM=18 µm.
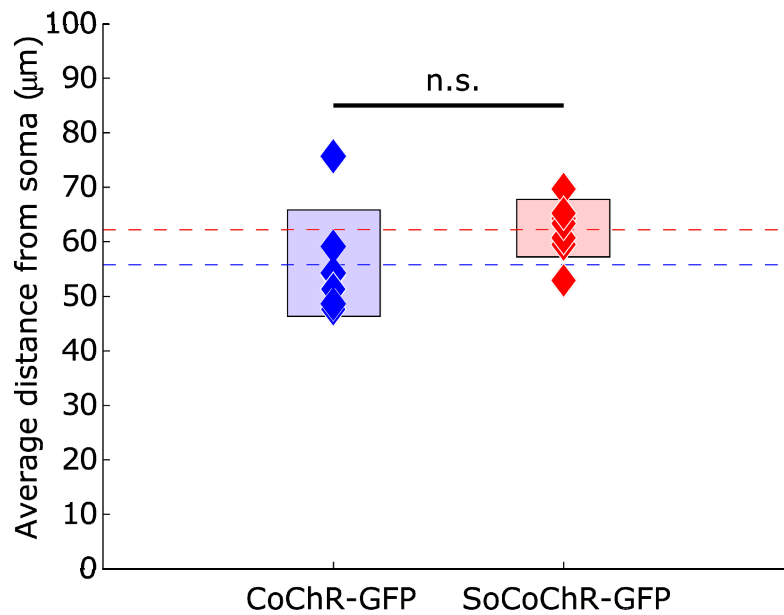
Supplementary Figure 12

Average distances between the soma of the patched cell and the somata of neighboring photostimulated cells.

This boxplot corresponds to experiments reported on **Fig. 5e,g**. Blue and red symbols represent average distances between the several photostimulated neighboring cells (n=5 to 8 cells) and the patched cells (7 patched cells expressing CoChR-GFP from 6 mice, blue symbols; 7 patched cells expressing soCoChR-GFP from 7 mice, red symbols). Horizontal dashed lines represent the average distance over all experiments (n=7 patched CoChR-GFP expressing cells, n=7 patched soCoChR-GFP expressing cells). The height of the rectangles represents two standard deviations of the distribution of the average distances over different experiments. The differences in the distances in the two groups were not significant under a Wilcoxon rank sum test. Statistics are reported in **Supplementary Table 4**.

a CoChR-GFP

Before synaptic receptor blockers: connection where (PSCs/ artifactual currents) > 1
Before synaptic receptor blockers: connection where (PSCs/ artifactual currents) < 1
No PSCs
In synaptic receptor blockers

Distance from patched cell (µm)

20 pA
50 ms

b soCoChR-GFP

Before synaptic receptor blockers: connection where (PSCs/ artifactual currents) > 1
No PSCs
In synaptic receptor blockers

Distance from patched cell (µm)

20 pA
50 ms

Supplementary Figure 13

Mapping of functional connectivity in brain slices.

(a) Currents recorded in whole-cell configuration from a CoChR-GFP expressing cell (same patched cell shown in **Fig. 6b**) while sequentially positioning the holographic spot on neighboring cells (λ = 920 nm, setup 2, photostimulation power: 120 µW/µm²; three light pulses at 50 Hz of 10 ms duration). Currents corresponding to neighboring cells numbered 3, 5 and 18 (green numbers) are shown in **Fig. 6**). The distances between each neighboring cell and the patched cell are reported next to each curve (grey numbers). Each trace is the average of three trials. Currents were recorded before the perfusion of synaptic receptor blockers (I_{TOT}) and after the perfusion of synaptic receptor blockers (I_{ART}). The current component sensitive to application of synaptic receptor blockers was: PSCs = I_{TOT} - I_{ART}. Black traces: I_{TOT} where the ratio PSCs/I_{ART} > 1. Gray traces: I_{TOT} where the ratio PSCs/I_{ART} <1. Red traces: I_{TOT} where no PSCs were observed (I_{TOT} = I_{ART}). Blue traces: I_{ART}. **(b)** Currents recorded in whole-cell configuration from a soCoChR-GFP expressing cell while sequentially positioning the holographic spot on neighboring cells (λ = 1030 nm, setup 1, photostimulation power: 120 µW/µm²; three light pulses at 50 Hz of 10 ms duration). Currents corresponding to neighboring cells numbered 6, 9 and 12 are shown in **Fig. 6**). The distances between each neighboring cell and the patched cell are reported next to each curve (grey numbers). Color code as in panel **(a)**.

Supplementary tables and supplementary notes

Supplementary table 1: soma-targeting candidate proteins

Name of protein	Was the protein fused to a fluorescent protein or an immunoepitope tag? If yes, was it an N-terminal or a C-terminal fusion? *	What was the soma targeting motif or peptide found?	Was the soma-targeting fragment fused to a fluorescent protein or an immunoepitope tag? If yes, was it an N- terminal or a C-terminal fusion? *	How far from the soma, approximately, was the fluorescence detected using visual inspection?	Did the sequence target an opsin to the soma or to the axon initial segment? If yes, what was the construct used?	Linker we used between CoChR and the localizati on sequence
Nav1.6	Yes. N-terminal with GFP [25]	Nav1.6(II-III) [25], a 27 amino acid sequence, from the intracellular loop between transmembrane domains II and III.	Yes. N-terminal [25] We made an N-terminal fusion.	Up to 20-70 μm	Yes, to the axon hillock; ChR2-GFP-Nav1.6(II-III) [30]	N/A
Nav1.2	Yes. N-terminal with GFP [25]	Nav1.2(II-III) [25], a 27 amino acid sequence, from the intracellular loop between transmembrane domains II and III.	Yes. N-terminal [25] We made an N-terminal fusion.	Up to 20-50 μm	Yes, to the axon hillock; ChR2-YFP-Nav1.2(II-III) [34]	ggsggt
Soma restricted proteolipid (srPLP)	No. The protein was labeled with antibodies [23] We made both N- and C-terminal fusions with GFP.	N/A	N/A	Up to > 100 μm	N/A	N/A
DM20	No. The protein was labeled with antibodies [23] We made both N- and C-terminal fusions with GFP.	N/A	N/A	Up to > 100 μm	N/A	N/A
Ankyrin_G	Yes. N-terminal with GFP [29]	Ankyrin_G(837) [31], from the N-terminal fragment of Ankyrin_G.	No. N-terminal fusions were made with ChR2 or with eNpHR [31]. We made both N- and C-terminal fusions.	Up to 20-50 μm The C-terminal fusion had a 10-fold higher expression than the N-terminal one.	Yes, to the soma. Ankyrin_G(837)-ChR2-mCherry and Ankyrin_G(1-2512)-eNpHR –GFP [31]. We made CoChR-Ankyrin_G(1-2512)-GFP which was somatic and enabled photostimulation in expressing neurons. Was not packaged in AAVs due to its large size.	ggsggt

L1-R184Q	Yes, N-terminal with GFP [26]. We made both N- and C-terminal fusions with GFP.	N/A	N/A	Up to 50-100µm	N/A	N/A
K$_V$2.1	Yes, a HA-tag was fused to the N-terminus of K$_V$2.1. [24].	K$_V$2.1-motif, a 65 amino acid sequence [30] from the C-terminal domain of K$_V$2.1.	No. C-terminal Fusions were made with ChR2 [30]. We made a C-terminal fusion with GFP.	Up to 60-150µm	Yes.. The expression of ChR2-YFP-Kv2.1-motif or NpHR-YFP-Kv2.1-motif[30] was somatodendritic. The expression of CoChR-GFP-Kv2.1-motif was somatodendritic (Figure S3).	N/A
KA2	Yes, a myc-tag was fused to the N-terminus of KA2. We made both N and C fusions with GFP.	KA2(1-150). To find it, we fragmented KA2 into (from N terminal to C terminal) into KA2_PART1 (360 amino acids), KA2_PART2 (360 amino acids) and KA2_PART3 (259 amino acids.	Yes, we made C and N terminal fusions of KA2(1-150) with GFP.	Up to 20-50 µm	Yes, to the soma. We cloned KA2(1-150)-CoChR-GFP (average current in expressing cells was 130 pA ± 34 pA), and CoChR--KA2(1-150)-GFP average current in expressing cells was 720 pA ± 156 pA) which was named soCoChR.	ggsggtggs ggt
BicD^{r5}	No, however FMRP was localized to the soma in neurons of fly larvae expressing BicDr5 [27].	Yes, in the BicD^{r5} allele there is a stop codon after the first 50 codons (out of 782) [28].	No. We made both N- and C-terminal fusions with GFP.	Up to > 100 µm	N/A	N/A

*N-terminal fusion means the organization of the final construct was: targeting_sequence-GFP or targeting_sequence-opsin, C-terminal fusion means the organization was: GFP-targeting_sequence or opsin-targeting_sequence.

Supplementary Table 2: Statistical analyses for Figure S1

<u>Figure S1d,e,f - GFP brightness versus position along a neurite, normalized to GFP brightness at the soma</u>

Two-sample Kolmogorov-Smirnov (K-S) tests with Bonferroni correction were performed, comparing normalized GFP brightness at different positions along neurites, across different constructs. The overall significance level α was set to 0.05, and the significance level of each individual K-S test was thus α/11 = 0.0045. P values less than 0.0045 are highlighted below in bold. For GFP, n = 5 neurites from 3 cells from 2 cultures. For KA2-GFP, n = 5 neurites from 3 cells from 2 cultures. For KA2(1-150)-GFP, n = 5 neurites from 3 cells from 2 cultures.

GFP vs. KA2-GFP:

Distance along neurite from soma (in microns)	0	10	20	30	40	50
p-value	0.6974	0.2090	0.0361	0.0361	0.0361	0.0361
Distance along neurite from soma (in microns)	60	70	80	90	100	-
p-value	0.0361	**0.0038**	0.0361	0.0361	0.0361	-

GFP vs. KA2(1-150)-GFP:

Distance along neurite from soma (in microns)	0	10	20	30	40	50
p-value	0.0361	**0.0038**	**0.0038**	**0.0038**	**0.0038**	0.0361
Distance along neurite from soma (in microns)	60	70	80	90	100	-
p-value	**0.0038**	0.0361	0.0361	0.0361	0.0361	-

KA2-GFP vs. KA2(1-150)-GFP:

Distance along neurite from soma (in microns)	0	10	20	30	40	50
p-value	**0.0038**	**0.0038**	0.2090	0.2090	0.0361	0.6974
Distance along neurite from soma (in microns)	60	70	80	90	100	-
p-value	0.6974	0.6974	0.6974	0.6974	0.6974	-

Supplementary Table 3: Statistical analyses for Figures 1, 2, S3 and S4

Figure 1m,n - GFP brightness versus position along a neurite, normalized to GFP brightness at the soma

Two-sample Kolmogorov-Smirnov (K-S) tests with Bonferroni correction for normalized GFP brightness at different positions along neurites, comparing across different constructs. The overall significance level α was set to 0.05, and the significance level of each individual K-S test was thus $\alpha/11 = 0.0045$. P values less than 0.0045 are highlighted in bold, below. For CoChR-GFP, n = 7 neurites from 5 cells from 2 cultures. For CoChR-KA2(1-150)-GFP, n = 9 neurites from 7 cells from 3 cultures. For CoChR-Nav1.2(II/III)-GFP, n = 5 neurites from 5 cells from 4 cultures.

CoChR-GFP vs. CoChR-KA2(1-150)-GFP:

Distance along neurite from soma (in microns)	0	10	20	30	40	50
p-value	**0.00018**	**0.00018**	0.01112	0.01714	0.01112	**0.00126**
Distance along neurite from soma (in microns)	60	70	80	90	100	-
p-value	**0.00221**	**0.00036**	**0.00213**	**0.00213**	**0.00213**	-

CoChR-GFP vs. CoChR-NaV1.2(II/III)-GFP:

Distance along neurite from soma (in microns)	0	10	20	30	40	50
p-value	0.2999	0.61557	0.2999	0.05179	0.01038	0.01038
Distance along neurite from soma (in microns)	60	70	80	90	100	-
p-value	0.01833	0.01833	0.05292	0.05292	0.2587	-

CoChR-KA2(1-150)-GFP vs. CoChR-NaV1.2(II/III)-GFP:

Distance along neurite from soma (in microns)	0	10	20	30	40	50
p-value	0.12085	0.12085	0.30923	0.30923	0.90097	0.56102
Distance along neurite from soma (in microns)	60	70	80	90	100	-
p-value	0.56102	0.56102	0.12085	0.56102	0.12085	-

Figure 1p – Photocurrent
Wilcoxon rank sum test for photocurrent values:

Molecule	# of cells
CoChR-GFP	13
CoChR-KA2(1-150)-GFP	13

P-value	0.6444
z-statistic	-0.4615
rank sum test statistic	166

Figure 1q - τ_{off}
Wilcoxon rank sum test for τ_{off} values:

Molecule	# of cells
CoChR-GFP	13
CoChR-KA2(1-150)-GFP	13

P-value	2.5928e-05
z-statistic	4.2066
rank sum test statistic	258

Figure 2c, d – distances of photostimulated neurons from the patched cell
The patched cell is cell #1

Cell #	Cell 2	Cell 3	Cell 4	Cell 5	Cell 6	Cell 7	Cell 8	Cell 9	Cell 10
Average distance from cell 1 in CoChR expressing cultures	24	36	42	82	76	108	80	116	128
s.e.m. of distance from cell 1 in CoChR expressing cultures	5	16	7	22	15	13	18	20	12
Average distance from cell 1 in soCoChR expressing cultures	16	32	44	74	80	92	82	120	128
s.e.m. of distance from cell 1 in soCoChR expressing cultures	2	5	16	17	6	10	10	18	14

Wilcoxon rank sum test for distances of photostimulated neurons from the patched cell:

Patched cells expressing:	# of cells	Distance of photostimulated cells from patched cell
CoChR-GFP	5	76.89 ± 6.98 µm
CoChR-KA2(1-150)-GFP	5	74.22 ± 6.50 µm

P-value	0.9488
rank sum test statistic	86.5000

Figure 2h –Percentage of photostimulated neighboring cells that yielded an AP in each patched cell

Wilcoxon rank sum test for photocurrent values:

Molecule	# of cells
CoChR-GFP	5
CoChR-KA2(1-150)-GFP	5

P-value	0.0476
rank sum test statistic	17.5

Figure 2i - percentage of photostimulated neighboring cells that yielded a depolarization in each patched cell

Molecule	# of patched cells
CoChR-GFP	5
CoChR-KA2(1-150)-GFP	5

Wilcoxon rank sum test of the percentage of photostimulated neighboring cells that yielded a depolarization in each patched cell, between CoChR-GFP and CoChR-KA2(1-150)-GFP:

P-value	0.0079
rank sum test statistic	15

Number of total depolarization events:

Molecule	# of depolarization events
CoChR-GFP	16
CoChR-KA2(1-150)-GFP	2

CoChR-GFP membrane potential increase (mV) in each depolarization event:

2	3	9	10	12	7	6	5
5	4	4	7	6	6	10	2

Average: 6.125mV

CoChR-KA2(1-150)-GFP membrane potential increase (mV) in each depolarization event:

4	6

Average: 5mV

Wilcoxon rank sum test of membrane potential increases in depolarization events between CoChR-GFP and CoChR-KA2(1-150)-GFP:

P-value	0.732
rank sum test statistic	15.5

Figure S3
Two-sample Kolmogorov-Smirnov (K-S) tests with Bonferroni correction for normalized GFP brightness at different positions along neurites, comparing across constructs. The overall significance level α was set to 0.05, and the significance level of each individual K-S test was thus $\alpha/11 = 0.0045$. P values less than 0.0045 are highlighted below in bold. For CoChR-GFP, n = 7 neurites from 5 cells from 2 cultures. For CoChR-GFP-Kv2.1$_{motif}$, n = 5 neurites from 5 cells from 2 cultures.

CoChR-GFP vs. CoChR-GFP-Kv2.1$_{motif}$:

Distance along neurite from soma (in microns)	0	10	20	30	40	50
p-value	0.0518	0.0518	0.5264	0.5264	0.5264	0.5264
Distance along neurite from soma (in microns)	60	70	80	90	100	-
p-value	0.8471	0.3670	0.4772	0.4772	0.4772	-

Figure S4 B – Blue light driven spike probability as a function of irradiance for CoChR-GFP and soCoChR-GFP expressing cells. n = 6 cells for each opsin.

Bonferroni-corrected Wilcoxon rank sum tests for spike probability at each irradiance, comparing across constructs. The overall significance level α was set to 0.05, and the significance level of each individual Wilcoxon rank sum test was thus $\alpha/6 = 0.0083$.

	1mW	2mW	3mW	5mW	7mW	10mW
P	0.909091	0.848485	0.242424	1	1	1
Ranksum	33	33.5	37.5	30	30	30

Figure S4 C – Blue light driven photocurrents as a function of irradiance for CoChR and soCoChR expressing cells. n = 7 cells for each opsin.

Bonferroni-corrected Wilcoxon rank sum tests for photocurrents at each irradiance. The overall significance level α was set to 0.05, and the significance level of each individual Wilcoxon rank sum test was $\alpha/6 = 0.0083$.

	1mW	2mW	3mW	5mW	7mW	10mW
P	0.600233	0.364219	0.710373	1	0.455711	0.534965
Ranksum	48.5	60	56	53	59	58

Figure S4 D – Blue light driven spike probability as a function of stimulation frequency for CoChR and soCoChR expressing cells. n = 7 - 10 cells for each opsin.

Bonferroni-corrected Wilcoxon rank sum tests for spike probability at each stimulation frequency. The overall significance level α was set to 0.05, and the significance level of each individual Wilcoxon rank sum test was $\alpha/5 = 0.01$.

	5Hz	10Hz	20Hz	40Hz	60Hz
P	1	0.823529	0.289593	0.07281	0.211024
Ranksum	63	58	51.5	45	51

Supplementary Table 4: Statistical analysis for Figure 3 and 5

Figure 3e – Normalized photocurrent integral generated by a photostimulation spot placed on neurites at different distances from the soma for CoChR-GFP and soCoChR-GFP expressing cells. The current integral is normalized to the current integral value obtained with the photostimulation spot at the soma.

Two-sample Kolmogorov-Smirnov test with Bonferroni correction for normalized integrated photocurrent for photostimulation along neurites. The current integral values were binned according to their distance from soma in intervals of 15 µm. The overall significance level α of the test was set to 0.05, and the significance level of each individual K-S test was α/6 = 0.0083. P values less than 0.0083 are highlighted in bold.

For CoChR-GFP, n=16 neurites from 8 cells from 7 mice.
For soCoChR-GFP, n=27 neurites from 16 cells from 13 mice.

Distance from soma along neurite (in microns)	0-Soma	15	30	45	60	75	90
n points per binning interval - CoChR-GFP	16	30	18	27	22	24	15
n points per binning interval - soCoChR-GFP	27	40	29	36	29	19	14
P-value	1	0.4627	**0.0006**	**0.0001**	**0.00001**	**0.0013**	**0.0002**

Percentage of photostimulation events, at a given distance from the soma along a neurite, for soCoChR expressing cells, generating a peak current lower than the lowest peak current induced among all the investigated neurites of CoChR expressing cells, and measured for stimulation at the same distance from the soma. Current peaks are evaluated on traces resulting from the average of 1 to 3 trials of photostimulation per site. The data correspond to the experiments reported in Fig. 3e and in Supplementary Figure S10.

Distance from soma along neurite (in microns)	15	30	45	60	75	90
% of photostimulation events at a given distance from soma along a neurite of soCoChR expressing cells generating a peak current lower than the lowest average peak current induced among all the investigated neurites of CoChR expressing cells at the same distance from the soma.	50	75	81	86	68	100

Figure 5e – Average distances of neighboring cells from the patched cell for CoChR-GFP and CoChR-KA2(1-150)-GFP expressing cells.

For each patched cell, the average distance across the neighboring stimulated cells is calculated. The resulting distances are then averaged over patched cells. Data are reported in Supplementary Figure S12.

A Wilcoxon rank sum test was performed between the average distances for the patched cells for CoChR-GFP and CoChR-KA2(1-150)-GFP expressing cells.

For CoChR-GFP, n=7 patched cells from 6 mice;
For CoChR-KA2(1-150)-GFP, n=7 patched cells from 7 mice).

Patched cells expressing:	# of cells	Distance of photostimulated cells from patched cell
CoChR-GFP	7	$55.7 \pm 9.6\mu m$
CoChR-KA2(1-150)-GFP	7	$62.2 \pm 5.3 \ \mu m$

P-value	0.0728

Figure 5e - Percentage of sequentially photostimulated neighboring cells that yielded action potentials in the patched cell.

Wilcoxon rank sum test for percentage values:

Molecule	# of cells
CoChR-GFP	7
CoChR-KA2(1-150)-GFP	7

P-value	0.004

Figure 5g - Percentage of simultaneously photostimulated neighboring cells that yielded one action potential in the patched cell.

χ^2-test:

Molecule	# of cells
CoChR-GFP	7
CoChR-KA2(1-150)-GFP	7

χ^2	3.97
df	1
P-value	0.046

Percentage of simultaneously photostimulated neighboring cells that yielded more than one action potential in the patched cell.

χ^2-test:

Molecule	# of cells
CoChR-GFP	7
CoChR-KA2(1-150)-GFP	7

χ^2	3.15
df	1
P-value	0.08

Supplementary Table 5: Statistical analysis for Figure 6

Figure 6c - <u>Comparison of artifactual mean peak currents when sequentially photostimulating neighboring cells</u>.
Wilcoxon rank sum test for percentage values:

Molecule	# of cells
CoChR-GFP	4
CoChR-KA2(1-150)-GFP	5

P-value	0.015

Figure 6d - Comparison of the PSC current/I_{ART} ratio when sequentially photostimulating neighboring cells..
Wilcoxon rank sum test for percentage values:

Molecule	# of cells
CoChR-GFP	4
CoChR-KA2(1-150)-GFP	5

P-value	0.003

Supplementary information

Amino acid sequence of KA2(1-150):

MPAELLLLLIVAFANPSCQVLSSLRMAAILDDQTVCGRGERLALALAREQINGIIEVPAK
ARVEVDIFELQRDSQYETTDTMCQILPKGVVSVLGPSSSPASASTVSHICGEKEIPHIKVG
PEETPRLQYLRFASVSLYPSNEDVSLAVS

Amino acid sequence of soCoChR:

MLGNGSAIVPIDQCFCLAWTDSLGSDTEQLVANILQWFAFGFSILILMFYAYQTW
RATCGWEEVYVCCVELTKVIIEFFHEFDDPSMLYLANGHRVQWLRYAEWLLTCPVILIH
LSNLTGLKDDYSKRTMRLLVSDVGTIVWGATSAMSTGYVKVIFFVLGCIYGANTFFHA
AKVYIESYHVVPKGRPRTVVRIMAWLFFLSWGMFPVLFVVGPEGFDAISVYGSTIGHTII
DLMSKNCWGLLGHYLRVLIHQHIIIYGDIRKKTKINVAGEEMEVETMVDQEDEETVGGS
GGTGGSGGTMPAELLLLLIVAFANPSCQVLSSLRMAAILDDQTVCGRGERLALALAREQ
INGIIEVPAKARVEVDIFELQRDSQYETTDTMCQILPKGVVSVLGPSSSPASASTVSHICGE
KEIPHIKVGPEETPRLQYLRFASVSLYPSNEDVSLAVSGASGGTVSKGEELFTGVVPILVE
LDGDVNGHKFSVSGEGEGDATYGKLTLKFICTTGKLPVPWPTLVTTLTYGVQCFSRYPD
HMKQHDFFKSAMPEGYVQERTIFFKDDGNYKTRAEVKFEGDTLVNRIELKGIDFKEDG
NILGHKLEYNYNSHNVYIMADKQKNGIKVNFKIRHNIEDGSVQLADHYQQNTPIGDGPV
LLPDNHYLSTQSALSKDPNEKRDHMVLLEFVTAAGITLGMDELYK